University of Alberta

Computer Simulation of Solid-Particle Erosion and Related Phenomena Using a Micro-Scale Dynamic Model

By

Qiang Chen

A thesis submitted to the faculty of Graduate Studies and Research in partial fulfillment of the requirements for the degree of Master of Science

In

Materials Engineering

Department of Chemical and Materials Engineering

Edmonton, Alberta

Spring 2003

National Library of Canada
Acquisitions and Bibliographic Services
395 Wellington Street
Ottawa ON K1A 0N4
Canada

Bibliothèque nationale du Canada
Acquisitions et services bibliographiques
395, rue Wellington
Ottawa ON K1A 0N4
Canada

Your file Votre référence

Our file Notre référence

The author has granted a non-exclusive licence allowing the National Library of Canada to reproduce, loan, distribute or sell copies of this thesis in microform, paper or electronic formats.

L'auteur a accordé une licence non exclusive permettant à la Bibliothèque nationale du Canada de reproduire, prêter, distribuer ou vendre des copies de cette thèse sous la forme de microfiche/film, de reproduction sur papier ou sur format électronique.

The author retains ownership of the copyright in this thesis. Neither the thesis nor substantial extracts from it may be printed or otherwise reproduced without the author's permission.

L'auteur conserve la propriété du droit d'auteur qui protège cette thèse. Ni la thèse ni des extraits substantiels de celle-ci ne doivent être imprimés ou autrement reproduits sans son autorisation.

0-612-82260-5

Canada

University of Alberta

Library Release Form

Name of Author: Qiang Chen

Title of Thesis: Computer simulation of solid-particle erosion and related phenomena using a micro-scale dynamic model

Degree: Master of Science

Year this Degree Granted: 2003

Permission is hereby granted to the University of Alberta Library to reproduce single copies of this thesis and to lend or sell such copies for private, scholarly, or scientific research purposes only.

The author reserves all other publication and other rights in association with copyright in the thesis, and except as herein before provided, neither the thesis nor any substantial portion thereof may be printed or otherwise reproduced in any material form whatever without the author's prior written permission.

Qiang Chen

Qiang Chen
3B 9108, Hub Mall
Edmonton, AB T6G 2C5

Date: Jan 3, 2003

University of Alberta

Faulty of Graduate Studies and Research

The undersigned certify that they have read, and recommend to the faculty of Graduate Studies and Research for acceptance, a thesis entitled Model Simulation of Solid-Particle Erosion of Homogeneous and Heterogeneous Materials submitted by Qiang Chen in partial fulfillment of the requirements for the degree of Master of Science in Materials Engineering.

Dongyang Li.

Dr.Dongyang Li, Supervisor

Reg Eadie

Dr.Reg Eadie, Committee Member

Dr.P-Y.Ben Jar, Committee Member

Date: Jan. 3, 2003

Abstract

Key words: Solid-particle erosion, Computer simulation, MSDM model

In this work, a micro-scale dynamic computational model (MSDM) was proposed to simulate the erosion process. It was developed based on Newton's law of motion. This model was applied to single-phase and composite materials. Influences of the shape, size, velocity and impact angle of solid particles on erosion were studied. In addition, effects of the reinforcing phase, the bonding strength of the reinforcing phase/matrix interface, the impact velocity, the solid-particle size and the size ratio of the solid-particle to the reinforcing phase on erosion of the composite were also investigated. The mechanisms responsible for the erosion behavior of both brittle and ductile materials are discussed. The model was also applied to simulate the indention process to investigate the interfacial bond strength and process of crack propagation in composite materials. Sliding wear was also modeled to investigate the influence of volume fraction of nano particles on sliding wear of a TiNi/TiC pseudoelastic composite.

Acknowledgment

First thank my supervisor, Dr D.Y.Li for his constant guidance and advice throughout this endeavor. His useful suggestions and innovative ideas have been of great assistance to me in completing this project.

I would also like to thank the staff members at the Department of Chemical and Materials Engineering for their assistance.

My special thanks are due to my colleagues in the Surface/Tribology Lab for their friendship and great help.

Finally, I am grateful for financial support from the Natural Science and Engineering Research Council of Canada (NSERC), Syncrude Canada Ltd. and Alberta Science and Research Authority (ASRA).

Table of Contents

Chapter 1 – Introduction and Literature Review

1.1 General introduction to wear.....2

1.2 Solid Particle Erosion.....5

1.2.1 Experimental techniques for erosion testing.....6

1.2.2 The development of models for solid-particle erosion.....9

Chapter 2 – Development of a micro scale dynamic model (MSDM) to simulate erosion of materials

2.1 Introduction.....21

2.2 Description of the micro-scale dynamic model.....21

- Determination of force on a lattice site.....22
- Influence of external force.....25
- The deformation of a system.....26
- Determination of the movement of lattice sites.....27
- Wear of a material.....28

2.3 The advantages and further development of MSDM.....30

2.4 Application of the MSDM in modeling erosive wear.....33

2.5 Summary.....40

Chapter 3 - Simulation of a solid particle erosion process for single-phase materials

Table of Contents

3.1 Simulation Procedure.....42

3.2 Simulation Results.....43

3.2.1 Effect of the erodent velocity on erosion.....43

3.2.2 Variations in erosion loss with respect to the impact angle.....44

3.2.3 Influences of the shape and rotation angle of the erodent particles on erosion...48

3.2.4 Crack propagation in brittle material.....51

3.3 Conclusion.....55

Chapter 4 - Simulation of a solid-particle erosion process for Composite Materials

4.1 Introduction.....58

4.2 Results and discussion.....60

4.2.1 Effect of the volume fraction of the reinforcing phase on erosion.....60

4.2.2 Effect of interfacial bonding in erosion.....61

4.2.3 Effect of erodent size on erosion.....65

4.2.4 Effect of the size ratio of the erodent to the reinforcing phase on erosion.....67

4.3 Conclusion.....69

Chapter 5 - Other Applications of the MSDM Technique

5.1 The application of MSDM in investigation of interfacial debonding.....72

Table of Contents

5.1.1 Introduction to an interfacial bonding test technique.....72

5.1.2 Experimental results.....74

5.1.3 Modeling of interfacial debonding.....76

5.1.4 Analysis of simulation results.....78

5.2 Simulation of abrasive wear of pseudoelastic Composite material with nano-particles.....84

5.2.1 Introduction.....84

5.2.2 Description of the modeling.....85

5.2.3 Simulation result.....88

5.3 Conclusion.....91

Chapter 6 - Conclusions and Future Work

6.1 Summary of the research results presented in different papers.....94

6.2 Future work.....97

1) Effects of multiple impact and erodent size distribution on erosion.....97

2) Effects of shapes of the reinforcing phase and erodent particles on erosion...97

3) 3-D model.....97

4) Determination of the time interval and initial length of bond.....98

5) Extension of MSDM technique for modeling other types of wear.....98

References.....100

List of Tables

Table 3.1 Mechanical properties of materials under study.....42

Table 5.1 Mechanical properties of the materials under study.....89

List of Figures

Fig.1.1 Schematic of some kinds of wear process.....4

Fig.1.2 (a) Slinger tester (b) Rotating arm tester (c) Nozzle.....6

Fig.1.3 The slurry –pot tester.....8

Fig.1.4 Schematic of an erodent particle traveling on a ductile metal surface.....10

Fig.1.5 Schematic of cross section of eroding metal surface.....12

Fig.1.6 The damage accumulation, computed by CDM for (a) 10,
(b) 100, (c) 200 impacts.....15

Fig.1.7 Relaxed atomic configurations for (a) a (110)[0 $\bar{1}$ 0] crack and (b)
a (110)[001] crack in different crystal structure.....18

Fig.2.1 Schematic of a two dimensional model for target material.....22

Fig.2.2 Schematic of stress-strain curve.....24

Fig.2.3 Illustration of the vectors used in equation for calculating
deformation.....27

Fig.2.4 The schematic of stress-strain curve for work hardening.....29

Fig.2.5 Schematic microstructure of 20%SiC-Al alloy.....30

Fig. 2.6 Variation of erosive mass loss rate of 430 and 304 stainless
steels with temperature for two erodent concentrations.....32

Fig.2.7 Melted and resolidified aluminum on a silicon carbide
erodent particle.....33

Fig.2.8 The sketch of the MSDM model for solid particle erosion.....34

Fig.2.9 Schematic illustration of tensile curves of ceramic and metal material.....36

Fig.2.10 The influence of Δt on the wear loss.....39

List of Figures (continued)

Fig.3.1 The influence of impact velocity on the erosion loss (ductile).....43

Fig.3.2 The influence of impact velocity on the erosion loss (ceramic).....43

Fig.3.3 The relationship between the impact angle and the erosion loss (ductile material).....45

Fig.3.4 The relationship between the impact angle and the erosion loss (brittle material).....45

Fig.3.5 Erosion of 1100-O aluminum relative to Al2O3 both impinged by SiC particles.....45

Fig.3.6 The surface morphology of ductile material after the impact by 30 erodent particles (a) impact angle = 30^0 and (b) impact angle = 90^0.....47

Fig.3.7 The surface morphology of brittle material after impact by 20 erodent particles (a) impact angle = 30^0 and (b) impact angle = 90^0.....47

Fig.3.8 Influence of the erodent shape on the erosion loss of ductile material under the impact of one sand particle.....50

Fig.3.9 Erosion losses of the ductile materials under the impact of one sand particle with different rotation angles.....50

Fig.3.10 Influence of the erodent shape on the erosion loss of ductile material under the impact of 50 erodent particles.....50

Fig.3.11 Erosion losses of the ductile material under the impact of erodent

List of Figures (continued)

particles with different rotation angles.....50

Fig.3.12 Simulation of crack propagation in the brittle material (The artificial erodent was used here).a) angle: 45^0 b) angle: 90^0 c) angle: 135^0.....53

Fig 3.13 Schematic illustration of crack growth under a spherical particle.....55

Fig 3.14 Schematic illustration of crack growth under a sharp tip.....55

Fig.4.1 The sketch of solid-particle erosion of a composite material.....59

Fig.4.2 Erosion loss vs the volume fraction of the reinforcing phase having different particle sizes.....60

Fig.4.3 Solid-particle erosion of composites with strong, medium and weak interfacial bonds.....62

Fig.4.4 The strengths of three interfacial bonds: σ_1 ____ strong bond, σ_2 ____ medium bond, and σ_3 ___ weak bond.....63

Fig.4.5 Erosion losses vs the volume fraction of the reinforcing phase for three different interfacial bonds.....64

Fig.4.6 Erosion of a composite caused by erodent respectively having three different particle sizes (under the same mass flow of the erodent).....66

Fig.4.7 Erosion of the composite for three size ratios (The volume fraction of the reinforcing phase was the same).....68

Fig.5.1 Schematic diagram of the indentation measurement.....74

Fig.5.2 Curves of load-time and lateral-time for brass/rubber bonding (a)

List of Figures (continued)

weak bonding (b) strong bonding (c) very strong bonding.....75

Fig.5.3 The target material and indenter are discretized.....77

Fig.5.4 The simulation results for the strong interface bond. (a) Final simulation figure of indentation. (b) Variations in lateral displacement of the indenter tip with time.....79

Fig.5.5 The simulation result for the middle interfacial bond. (a) Final simulation figure of indentation. (b) Variations in lateral displacement of the indenter tip with time.....80

Fig.5.6 Interfacial failure during indentation.....82

Fig.5.7 The simulation result for the weak interfacial bond. (a) Final simulation figure of indentation. (b) Variations in lateral displacement of the indenter tip with time.....83

Fig.5.8 The Pseudoelasticity of TiNi alloy.....84

Fig.5.9 The schematic of a two-dimensional model for nano-TiN/TiC/TiNi Composites.....86

Fig.5.10 the schematic of four stages of stress-strain curve of pseudoelastic TiNi matrix.....88

Fig.5.11 Sliding wear with different nano-TiN content.....91

Fig.5.12 Volume losses of TiC/TiNi composites with different volume fractions of nano-TiN particles.....91

Fig.6.1 A flow chart of the MSDM.....96

Chapter 1

Introduction And Literature Review

1.1 General Introduction to Wear

Wear is defined by the American Society for Testing and Materials (ASTM) as the damage to a solid surface, generally involving the progressive loss of material, due to relative motion between two surfaces in contact [1]. Wear may also occur when the surfaces of engineering materials are in relative rolling motion [2]. Along with friction and lubrication, wear can be regarded as a subject of the science and technology of interacting surfaces, which is called tribology.

Wear is a complex surface-damage process, involving time-dependent deformation, failure and removal of materials at the counter-face. Wear does not only result in high costs for repair or replacement of failed machinery and equipment, but also the costs for the lost production. Although it is a surface destructive process, wear may lead to failure of a mechanical component or even an entire system. In North America, it has been estimated that wear and friction cost Canada in excess of $5 billion per year and cost U.S.A more than $100 billion per annum [3,4]. Considerable efforts have been made to investigate wear phenomena. For example, Meng and Ludema have identified nearly 200 wear equations involving enormous numbers of materials properties and operating conditions [5]. However, despite considerable research efforts, there are no effective analytic methods, which can be used to predict the tribological performance of a specific surface, even if its physical and chemical properties are known.

Wear may occur in different modes. The following are the most common wear modes encountered in industry, including abrasive wear, erosive wear, impact wear,

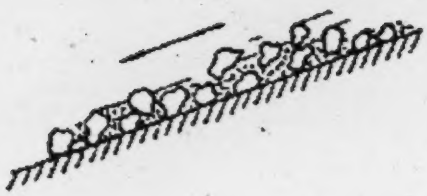

(a) Low-stress abrasion

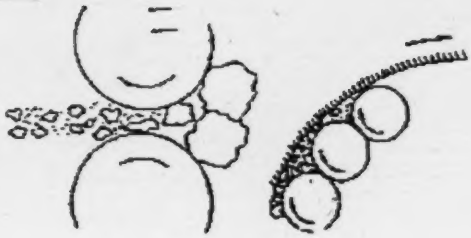

(b) Three-body abrasion

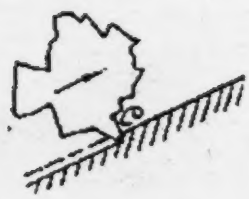

(c) Two-body abrasion

(d) Erosion, or corrosion-erosion

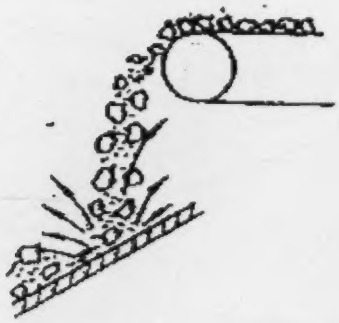

(e) Impact wear

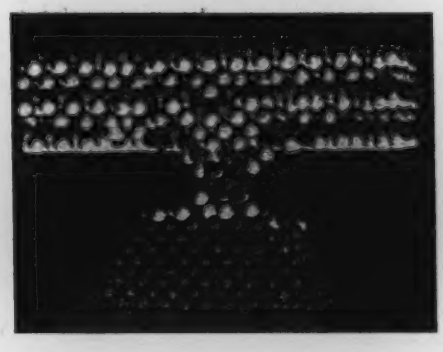

(f) Adhesive wear

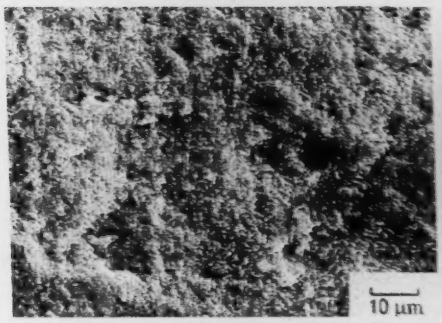

(g) Oxidative wear (h) Fatigue wear

Fig.1.1 Schematic of some kinds of wear process

corrosion-erosion, corrosive wear, adhesive wear and fatigue wear. Fig.1.1 (a) shows the abrasion under low stress. In this case, particles move parallel to the surface with low stress introduced in the target surface layer. If high stress exists, the particles will cut and plow the surface (Fig.1.1(c)). Another kind of abrasion is three-body abrasion. With this mode, particles are pressed between two surfaces moving in opposite directions (Fig.1.1 (b)). Erosion is always generated when small particles impinge the surface of a material, as shown in Fig.1.1 (d). Impact wear (Fig.1.1 (e)) is similar to erosion, except that the size of erodent for impact wear is larger than that of erodent for erosion. For adhesive wear, the adhesion of atoms between two materials plays an important role, just as illustrated in Fig.1.1 (f). Corrosive wear is also a common wear mode. In this process, sliding takes place in a corrosive environment. Besides, electrochemical reactions occur at the surface simultaneously, as illustrated in Fig.1.1 (g). Another wear mode is fatigue wear, which results from the repetitive action of the counter-bodies under a cyclic load (Fig.1.1 (h)).

Erosion is a very important wear mode in industry, especially in the oil sand mining systems. Solid-particle erosion is one of the most important erosion modes.

1.2 Solid-particle erosion

Solid-particle erosion occurs when a surface is attacked by impingement of solid particles. Solid-particle erosion occurs on the surfaces of exposed components in many different types of equipments, e.g. erosion of pipelines, pumps and screens. It may also occur in conjunction with other wear modes, such as abrasive wear, and under environmental influences such as the effects of corrosive solutions and elevated temperatures. An erosion process of a material is dependent on many interrelated factors that include properties and structures of the target material and the solid particles, the surface condition of the target material, and the geometry of the particles. The number of influencing factors may exceed twenty. Therefore, it is difficult to precisely predict the process of particle impacting erosion based on experiments and theories.

Considerable efforts have been made to understand erosion processes. Two relatively simple mechanisms make up of the essence of small solid-particle erosion. On a ductile material, the impacting particles cause severe localized plastic deformation that eventually exceeds the critical strain at fracture of the target material. On a brittle material, the force of erodent particles causes brittle cracking and chipping of the target material.

1.2.1 Experimental techniques for erosion testing

In order to select and design effective materials to resist erosion in industry, the performance of material during erosion need to be evaluated. Several types of apparatuses are widely used for solid-particle erosion tests [6]. They are the

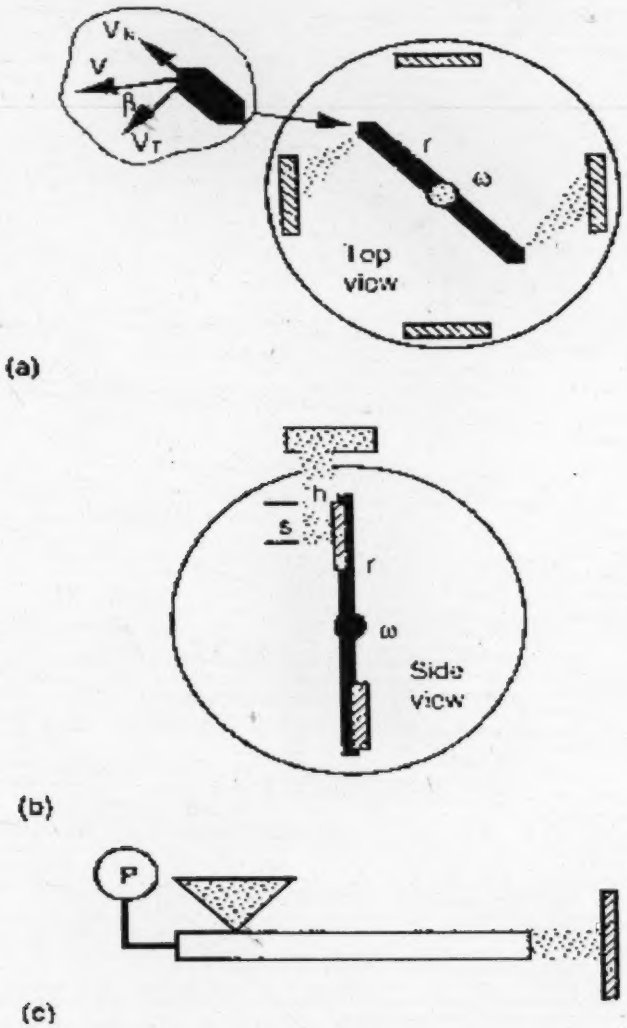

Fig.1.2 (a) Slinger tester (b) Rotating arm tester (c) Nozzle tester

slinger tester, rotating arm and the nozzle erosion tester. Fig.1.2 is a schematics of these testers. The slinger system feeds particles into the center of a rotating barrel in a chamber, whereupon they accelerate outward and exit from the barrel ends. Multiple samples can be arranged around the inner circumference of the chamber. This is an advantage when compared with the other two systems. The chamber must be under vacuum in order to avoid hydrodynamic losses.

In the rotating arm apparatus, samples are mounted on the rotating arm. Erodent particles are introduced as shown in Fig.1.2 (b) and allowed to free-fall a distance h before being intercepted by the rotating samples. Vacuum may be needed for an erosion test. The advantage of this system is the easy control of the erodent velocity by adjusting the rotating speed of the arm. In addition, a wide velocity range is permitted.

The nozzle tester is widely used in laboratories and in industries as well. A jet of pressurized gas is used as a carrier to accelerate the particles through the nozzle tube, whereupon they exit and impact a single target sample. The tester can be oriented either horizontally or vertically. The particle velocity can be varied by changing the air-pressure head. Vacuum chamber is not needed here.

Another type of erosion tester is the slurry-pot tester. As Fig.1.3 describes, several samples can be held on a rotating frame in the container. A slurry, which consists of a fluid and solid particles or pure solid particles, is put into the container. The surface of the slurry in container should be higher than the position of samples. During testing, the samples rotate driven by a rotating arm and collide with the slurry. By the interaction with slurry, surfaces of the samples are damaged and the wear loss is measured. The impact angle and contact surface can be controlled by adjusting the mounting angle and

position of the samples. The impact velocity can be varied by changing the rotating speed of the rotating arm.

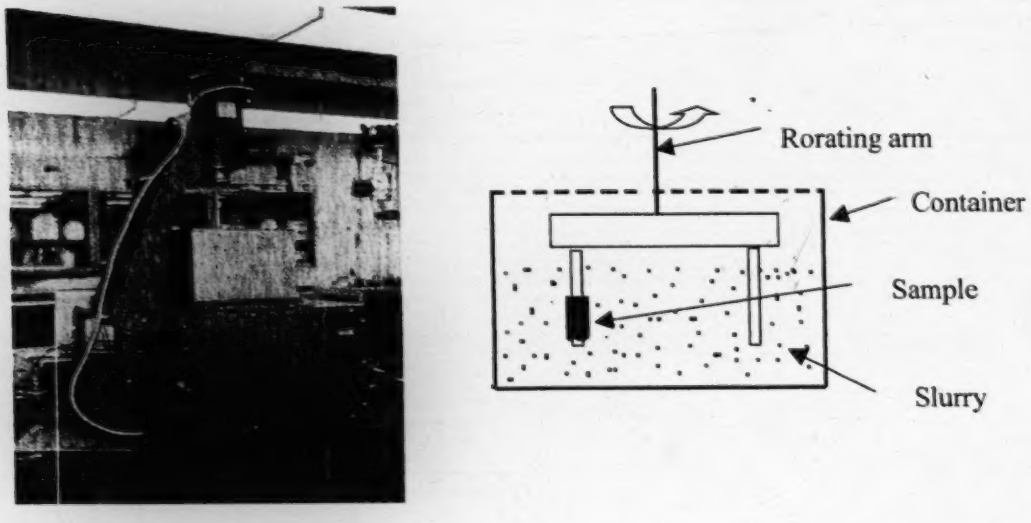

Fig.1.3 The slurry –pot tester

The above-mentioned testers are often used to evaluate the performance of a material under attack by erodent. Information about the effect of the velocity of sand on wear loss of the target material, the effect of the impact angle of sand on the erosion rate, and the relationship between the sand size and the erosion rate etc., could be determined by performing erosion tests. However, the erosion test may not give explicit clues to crucial factors that determine the erosion process of materials, having different microstructures and mechanical properties. In addition, the data obtained from the erosion test may not be sufficient to explain the mechanisms that are responsible for erosion under different conditions. Therefore, better approaches are necessary in order to

fundamentally understand the mechanisms for various processes of solid-particle erosion and the governing factors.

1.2.2 The development of models for solid-particle erosion

As shown earlier, a solid-particle erosion process is affected by many factors, such as the contact geometry, the mechanical properties of the surfaces in contact, the microstructures of the materials involved and the loading condition, etc. Obviously, it is difficult to theoretically predict erosion with accuracy. It is also difficult to clarify mechanisms responsible for solid-particle erosion through theoretical and experimental approaches. A promising method is computer simulation. Computer simulation provides an effective and economical approach, which allows the investigation of effects of different factors on erosion under controllable conditions. Each parameter involved in solid-particle erosion process can thus be studied separately.

Since 1958, when an erosion model for ductile metals was proposed by Finnie [7], a number of papers on erosion of metals by solid particles, ingested sand in helicopter engines and several other applications were published [8-14]. These models were based on a cutting mechanism, in which the motion equations of the particles were used to describe the process of erosion. The model that Finnie built [8] was based on the assumption that individual erodent particles traversed along the surface of the target metal and a chunk of metal was cut out as Fig.1.4 shows. The volume of material removed was calculated from the trajectory of each particle and the amount of cutting that would occur as a result of pure plastic deformation with no cracks propagating ahead

of the erodent particle. In the model, the equations that describe motion of the sand particles and thus the occurrence of erosion were expressed as follow:

$$Q = \frac{MV^2}{2P}(\sin^2\alpha - 3\sin^2\alpha)$$
$$\alpha \le 18.5^0 \qquad (1.1)$$

$$Q = \frac{MV^2}{24P}\cos^2\alpha$$
$$\alpha \ge 18.5^0 \qquad (1.2)$$

Where Q = the removed volume of the target material, M = the mean mass of angular particle, V = the particle velocity, P = the plastic flow stress, and α = the impingement angle.

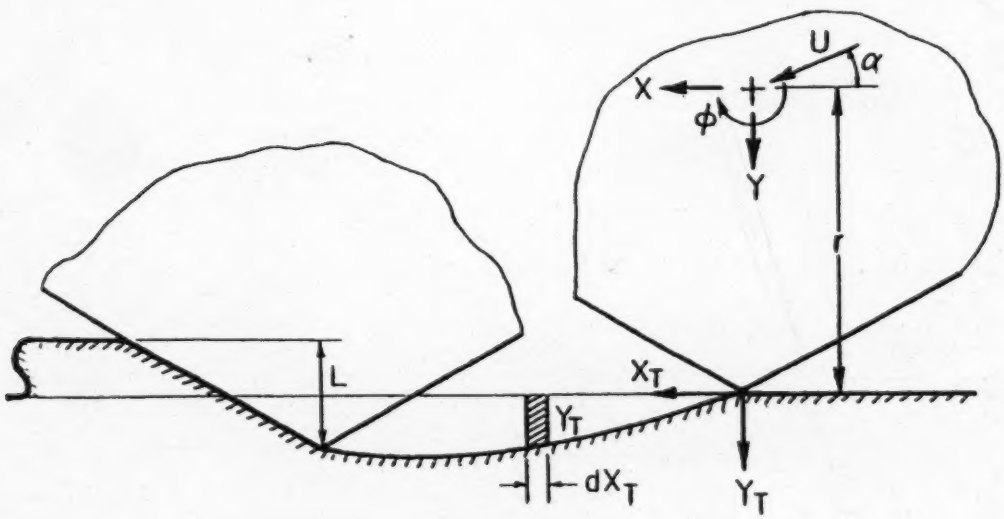

Fig.1.4 Schematic of an erodent particle traveling on a ductile metal surface

Results obtained using the Finnie's approach are consistent with those from erosion tests. In the model, some properties of sand and target material are considered, such as the mass of angular particles and plastic flow stress of the target material. However, some important properties are ignored in the model, such as the ductility and microstructures of the materials. As a result, the Finnie's approach and models built on this approach are rather limited for engineering design and fundamental understanding.

In 1975, significant progress was made in the study of solid-particle erosion when the scanning electron microscopy began to be used to examine the eroded surface. The morphological observation by SEM made it possible to investigate the mechanism responsible for erosion damage. The results showed that the erosion of a metal is primarily an extrusion, forging and fracture process but not a microcutting process as Finnie suggested. Based on the SEM observation, Hutchings proposed a new mechanism, the so-called platelet mechanism [15]. In the model a criterion of critical plastic strain is employed to determine when material is removed. The mechanical behavior of a metal was described mainly by two quantities: the dynamic hardness of the metal and its ductility under the erosion conditions. The equation can be expressed as:

$$E = 0.033 \frac{\alpha \rho \sigma^{1/2} v^3}{\varepsilon^2{}_c P^{2/3}} \qquad (1.3)$$

where E is the mass loss from the target surface per unit mass of erodent particles, α is half the dynamic indentation length of sand, ρ is the density of the material, σ is the density of sand, P is the plastic flow stress, and ε_c is the erosion ductility.

The dynamic hardness of a metal may be calculated from result of indentation made by single-sphere impact at a specific velocity and is therefore amenable to

independent measurement, but the erosion ductility is not readily measured and has to be derived, together with the ratio α, from experimental measurements of the erosion rate.

Levy further investigated this mechanism [16,17]. Fig.1.5 shows the schematic of cross section of an eroded metal surface. The erosion surface consists of platelets as the result of large plastic strain deformation. Beneath the surface is a work-hardened zone formed during the early stages of erosion. The strain-hardening depends on a function of the strain-hardening coefficient of the target metal. Under this zone is the base metal uninfluenced by erodent particles.

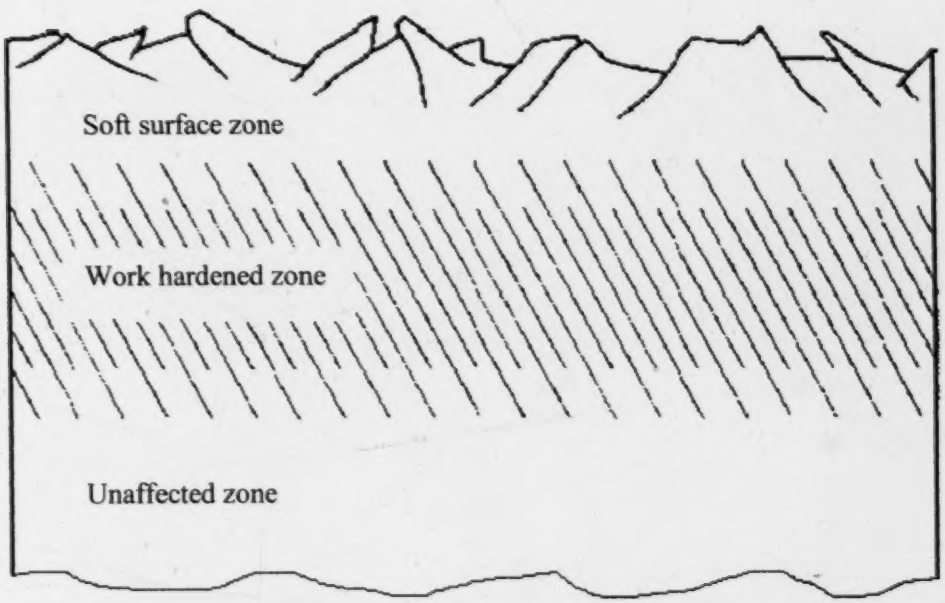

Fig.1.5 Schematic of cross section of eroding metal surface

Compared with the microcutting mechanism, the platelet mechanism is much better due to the introduction of work hardening of the materials. This means that the plastic

deformation and work hardening of the target material should be considered when building the model to simulate an erosion process. But the models based on the platelet mechanism still depend on some experimental results, such as the erosion ductility ε_c. Microstructure of material is also not considered in the model.

The most widely used method for modeling solid-particle erosion is the finite element method (FEM). In this method, a material system is meshed and represented by many unit elements. Each unit element is analyzed and a stiffness matrix is calculated. By assembling all of the elements composed of the material system and adding the boundary conditions such as the load and constrains, wear could be investigated [18-20]. For example, using the Tabor theory and a general-purpose structure-analysis software (MARC) based on the finite element method, Shimizu [20] analyzed the collision angle dependence of plastic deformation caused by a solid particle. Recently Woytowitz used this method to simulate impact on surface of a kinetically hardening, elastic-plastic material [21,22]. A 2D and 3D FE model with multiple impact spheres is developed, which can describe spatial and temporal accumulation of damage. In this model a strain-life approach with rainflow counting, a method based on cyclic plastic work (CPW) and a method based on a continuum damage mechanism (CDM) are used to simulate the erosion process with multiple impacts. Fig.1.6 illustrates the damage accumulation computed by CDM for 10, 100 and 200 impingements. In terms of the wear rate with time and sand velocity, the results from a simulation using FEM showed similar rules as those from experiment. This model has advantages over others because it includes the mechanical properties, work-hardening and especially multiple non-coincident impact (in the previous models, only the influence of one particle was considered and other particles

were treated as the same as the first one). In addition, some mechanisms of erosion, for example, cyclic deformation, can be analyzed using this method. But when calculating the wear loss, it uses an average damage over entire surface, which may lead to error. This model, at present stage, does not take into account of microstructural effects on erosion, which is crucial to material design and selection. In addition, the failure process during erosion is not well revealed by the model so that it is difficult to gain an insight into the damage mechanism.

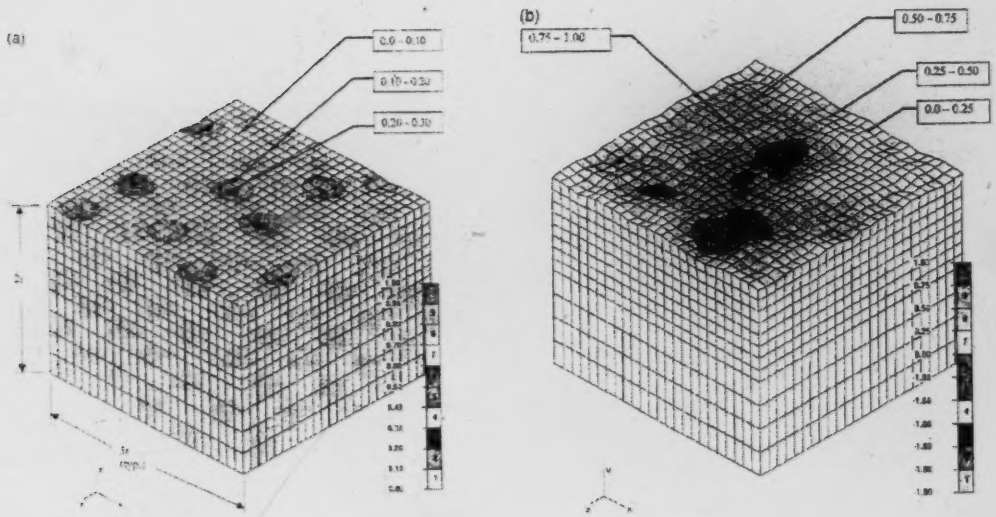

(a) (b)

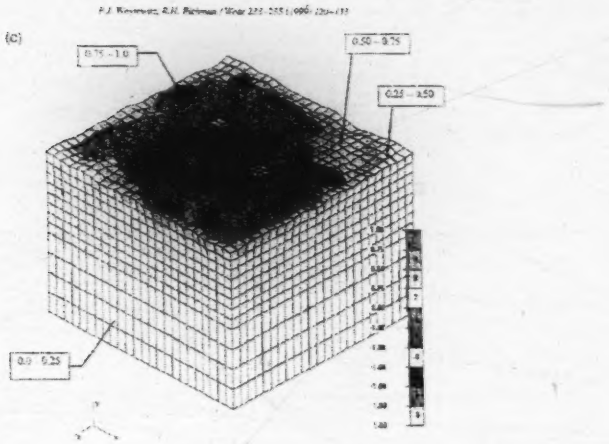

(c)

Fig.1.6 The damage accumulation, computed by CDM for (a) 10, (b) 100, (c) 200 impacts

The finite element method is effective for analyzing the distribution of stress/strain. However, application of FEM is limited and has difficulty in precisely predicting fracture and cracking direction. For a solid-particle erosion process, a dynamic process involves cracking, mass loss, and changes in surface properties and morphology. Hence it is difficult to use the finite element method to simulate such a process.

Erosion of ceramics and other low ductility materials is much different from that of ductile materials. For low ductility materials, their work hardening is very small and has little influence on the erosion process. That makes it simpler to simulate erosion of brittle materials. There are two representative models proposed for modeling erosion of brittle materials; one is built based on the assumption that erosion is a result of crack propagation and chipping [23]. Another model is proposed based on the assumption that

plastic deformation is involved in the process of crack formation and surface chipping [24].

All the above-mentioned models were developed on macro-level scales and therefore are not suitable for simulation of heterogeneous materials such as composites affected by microstructure. There are also other models proposed to simulate solid-particle erosion process [25,26]. To some extent these models provide information that is consistent with experiment observations. However, these models were developed based on existing tribological rules such as Archard's equations [27] or empirical equations such as Finnie's microcutting wear equation [7] and Hutchings' fatigue wear equation [15]. Therefore, the models may not be suitable for investigating erosion mechanisms and microstructural effects on erosion. The finite element method can be used to solve elastic/plastic contact problems in two-dimensional and three-dimensional spaces. However, this method does not take into account of the removal of elements and has difficulty to describe dynamic failure process. FEM analysis is also restricted to the simulation of a limited number of asperities due to limited computing capability. For a rough surface, a large number of meshing elements are required and this makes the FEM difficult to be used to simulate erosion process.

Further efforts have been made to build an effective model to simulate the process of solid-particle erosion. Since erosion is such a complex process, no model has been widely accepted. Ludema [28] reviewed ninety-eight mathematical models reported in literature. He indicated that none of them were accurate enough to predict the erosion process.

Considerable efforts have also been made to model wear processes on the atomistic level employing fundamental physics laws. Molecular Dynamic Simulation technique is the most powerful one. The principle of MD simulation is simple. In this method Newton's equation of motion is used to predict the trajectories of atoms [29].

$$\vec{F} = m \frac{d^2 \vec{r}}{dt^2} \tag{1.4}$$

where m is the mass of an atom, $\vec{r}$ is the position of the atom and t is the time, $\vec{F}$ is the total force on the atom, including the interaction between the atom and its neighbors as well as any external influence if the atom is at surface under external force.

After the force on each atom is calculated and determined, the movement of each atom can be determined using Newton's law, so that a new position of the atom can be determined after a time interval Δt. The MD method has been successfully applied in many fields, such as fracture, solidification, interface and nano-structure of materials [30, 31]. Fig.1.7 illustrates two cracks in two different crystals.

The main advantage of the MD method is that the positions of all atoms can be determined, so that one may investigate a particular dynamic process for fundamental understanding. When this method is used to simulate a wear process, we can judge whether an atom is worn away by calculating its position. As a result, a dynamic wear process can be simulated and resultant wear loss can be calculated. The MD method has been applied to simulate adhesive wear and friction [32].

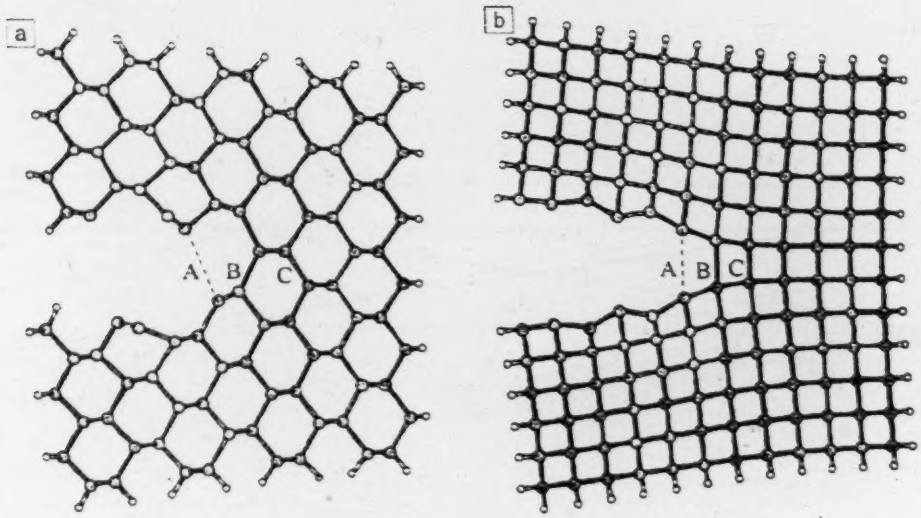

Fig.1.7 Relaxed atomic configurations for (a) a (110)[0 $\bar{1}$ 0] crack and (b) a (110)[001] crack in different crystal structure.

The molecular dynamic simulation method provides a powerful tool because it is developed based on the fundamental physical laws. Therefore, this method, in general, does not depend on experimental input. However, it is difficult to apply this method to a wear process because of the calculation limitation of computer. The molecular dynamic approach is often used to simulate a process involving 10^3~10^4 atoms and is therefore better for nano-level wear processes. In order to obtain meaningful result, a large number of atoms must be taken into account when simulating a wear process. For instance, to simulate a material system with its volume equal to $1um^3$, 10^9~10^{10} atoms should be calculated. Obviously it is not feasible to apply the MD method to simulate the process of solid-particle erosion with current computing capability. Nevertheless, the MD method is

the most promising technique, which would eventually become an industrial tool when our computing capability is significantly improved.

Considering the advantages and disadvantages of various models, great efforts have continuously been made to develop effective and realistic modeling approaches to simulate tribological processes and material behaviors. Recently, a tentative dynamic approach, the so-called Micro-Scale Dynamic Model (MSDM) was developed to simulate abrasive wear [33-35]. This model takes advantages of the MD technique and macro-models, thus making it possible to simulate a dynamic wear process on micro- and macro- scales. It has been demonstrated that this model can be used to simulate abrasive wear of materials with different microstructures and it provides meaningful predictions consistent with experimental observation. In the present work, a computer model was developed based on the MSDM to simulate erosion of homogeneous and heterogeneous materials.

Chapter 2

Development of a micro scale dynamic model (MSDM) to simulate erosion of materials

2.1 Introduction

In this work, an erosion model was developed from the micro-scale dynamic model (MSDM) based on the molecular dynamic technique. Because the MD method can only be used to model a limited number of atoms, it is difficult to apply it to simulate a wear process involving micro structural effect. The MSDM takes advantage of MD and also employs Newton's law of motion: $\vec{F} = m \frac{d^2 \vec{r}}{dt^2}$. The main difference between the MSDM and the MD come from the following factors: (1) the former deals with small volumes or blocks of materials while the latter deals with individual atoms; and (2) in the MSDM, the interaction between a pair of adjacent volumes of material is a function of the mechanical properties of the material while that between atoms for the MD modeling is determined by an atomic potential.

Micro-scale dynamic modeling inherits the advantages of the molecular dynamic technique with the capability of modeling wear of materials with specific microstructures on micro- or macro-scales.

2.2 Description of the micro-scale dynamic model

The present simulation is performed in a two dimensional space. In this model (MSDM), a given specimen is discretized using a square lattice (see Fig.2.1). Each site of which represents a small volume of the material. In the initial state, no interaction exists between adjacent sites. Under the influence of external force during a wear process, a lattice site may move, depending on the force on the site. The total force includes the

interaction between the site and its neighbors and external stress if the site is at the surface under external force. If the mechanical properties of the material and loading condition are given, the wear process can be determined.

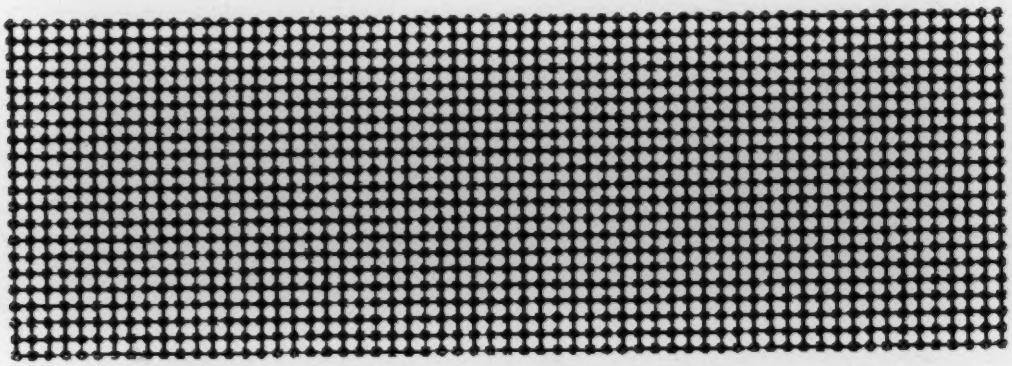

Fig.2.1 Schematic of a two dimensional model for target material

An important issue in this model is the determination of the total force on each lattice site. Here some techniques will be used to calculate the force. Details of the force calculation are given in the following section.

Determination of force on a lattice site

When a force is exerted on a lattice site, the movement and trajectory of the site is determined by Newton's law of motion:

$$\vec{F} = m \frac{d^2 \vec{r}}{dt^2} \tag{2.1}$$

where m is the mass of a lattice site, $\vec{F}$ represents the total force exerted on the lattice site, $\vec{r}$ is the position of the site. This force is the sum of all of the forces including the

interaction between the site and its adjacent sites, and external force, if it is exerted on this site.

The total force on a lattice site is expressed as:

$$\vec{F}_p = \sum_1^n k \cdot \Delta \vec{l}\,(p, m) + \vec{f}_p \qquad (2.2)$$

where n is the number of sites adjacent to this site, k is the coefficient, which equals to $E \cdot l_0$, $\Delta \vec{l}$ is the deformation of the bond under the stress, E is the modulus of the material and l_0 is the length of bond between two adjacent sites in stress-free condition. The first term is the interaction between the site and its adjacent sites. The second right term is an external force on the site if the site is at surface under external mechanical action.

The interaction between two adjacent sites is dependent on the mechanical properties of the material, which include the elastic modulus, the yield stress, the tensile strength, the ductility and work hardening. The interaction between two adjacent sites can be writen as:

$$\vec{f} = k \cdot \Delta \vec{l} \qquad (2.3)$$

here $\Delta \vec{l}$ is the deformation of the bond under the stress. It can be calculated by subtracting the stress-free bond length from the bond length after deformation under the force: $\Delta \vec{l} = \vec{l} - \vec{l}_0$. The coefficient k is equal to $E \cdot l_0$, where E is the slope of the stress-strain curve of the material. Fig.2.2 shows the schematic of a stress-strain curve. Within the elastic region, the curve is a linear, corresponding to the elastic modulus *Ee* while in plastic region the "modulus" varies with the strain. In order to

simplify the model, we use the slope of the line between the two points, defined as the plastic modulus. In the elastic region, $E = E_e = \sigma_y / \varepsilon_y$, where σ_y and ε_y are the yield stress and yield strain, respectively. In the

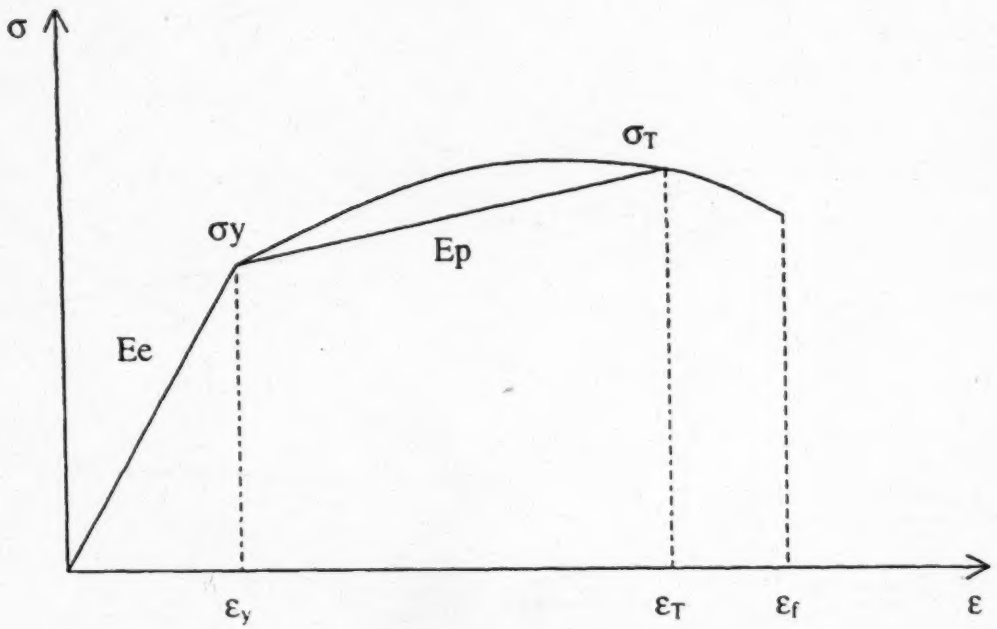

Fig.2.2 Schematic of stress-strain curve

plastic region, $E = E_p = (\sigma_T - \sigma_Y) / (\varepsilon_T - \varepsilon_Y)$. If the deformation Δl is within the region of elasticity, E is equal to the elastic modulus (E_e); if the deformation Δl exceeds the elastic region, E is equal to the plastic modulus (E_p). When the deformation Δl is smaller than zero, two sites are under compression. In this case, we assume E is equal to the elastic modulus and no damage to the bond will result. Similar to

the interaction between two atoms, the site-site bond will not be broken when the sites approach to each other under the compressive stress. Only when the bond is elongated and its deformation is larger than the strain at fracture, the bond will be broken.

Influence of external force

When a target surface is in contact with another one, the interaction occurs between the surfaces. The force due to the contact is transferred to the lattice sites through the surface of the target material, resulting in the deformation and fracture of the target material. In order to calculate the external force, the material that is in contact with target material also needs to be discretized. Consequently we may consider the external force as the interaction among the sites of the target material and those moving relative to the former. Because there is no bond between the sites of these two bodies in contact, no tension but only compression results. As described earlier, under compression the deformation of a site-site bond is assumed to be only elastic. The interaction between two sites respectively at the surfaces of the target surface and its opposite is determined. Assuming that the force coefficient of the target material (e.g., a metal) is k_m and that of the other (e.g., a sand particle) is k_s, the force between a pair of the metal and sand may be expressed as:

$$f = k_s \cdot \Delta l_s = k_m \cdot \Delta l_m \tag{2.4}$$

where m is referred to the target material, while s is referred to the other surface that slide on the target surface. Δl_s and Δl_m are half the deformations of a metal bond and a sand bond, respectively. The total deformation between these two sites is:

$$\Delta l = \Delta l_s + \Delta l_m \tag{2.5}$$

The force f can thus be derived from equation (2.4) and (2.5)

$$f = \bar{k} \cdot \Delta l = \bar{k} \cdot (\Delta l_s + \Delta l_m) = \bar{k} \cdot (\Delta l_s + \frac{k_s}{k_m} \Delta l_s) = k_s \cdot \Delta l_s \qquad (2.6)$$

where $\bar{k}$ is the effective force coefficient for the bond between two different sites. We may derive from equation (2.6) that

$$\bar{k} = {k_s k_m}/{(k_s + k_m)} \qquad (2.7)$$

The external force can thus be represented as

$$\bar{f}_p = \sum_1^m \bar{k} \cdot \Delta \vec{l} \qquad (2.8)$$

m is the number of sites adjacent to a particular site under study.

The deformation of a system

In order to calculate the total force on a site, we should know the position of each site first. The total deformation of a bond is equal to the length of the deformed bond after subtracting its stress-free length. If Δl (Δl is the absolute value of $\Delta \vec{l}$) is larger than zero, the bond is in tension; otherwise the bond is in compression. For two sites without bonding (e.g., the interaction between a metal site and a sand site when they are in contact), there is only

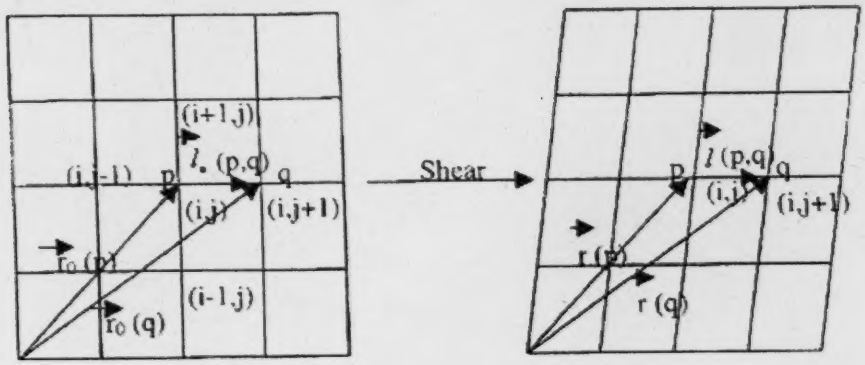

Fig.2.3 Illustration of the vectors used in equation for calculating deformation

compression i.e. Δl is smaller than zero, where Δl is the total deformation between the two sites. In general, Δl is expressed by the following equation:

$$\Delta\vec{l}(p,q)=\vec{l}(p,q)-\vec{l}_0(p,q)=[\vec{r}(q)-\vec{r}(p)]-\vec{l}_0(p,q) \qquad (2.9)$$

where $\Delta\vec{l}_0(p,q)$ is the vector of the bond between sites p and q in the stress-free state; $\vec{r}(p)$ is the position vector of site p and $\vec{r}(q)$ is the position vector of site q. All the vectors in the equation are labeled in Fig.2.3.

Determination of the movement of lattice sites

If Δl is known, the force on a site can be calculated using equation (2.2).

The movement of lattice sites can be consequently determined using Newton's law of motion. Initially, there is no deformation in a system i.e. the length of all site-site bonds are equal to l_0, if no stress exists in the system. If the position and velocity of the site at the time t are known, the new position and velocity of all the sites after a small

time interval Δt can be determined when the system is under the external force. The new position and velocity of each site are determined using the following equations:

$$\vec{V}_{t+\Delta t}(p) = \vec{V}_t(p) + \frac{1}{m}\vec{F}_t(p)\Delta t \tag{2.10}$$

$$\vec{r}_{t+\Delta t}(p) = \vec{r}_t(p) + \vec{V}_t(p)\Delta t \tag{2.11}$$

Here $\vec{V}_t(p)$ and $\vec{r}_t(p)$ are respectively the velocity and position of site p at the time t, while $\vec{V}_{t+\Delta t}(p)$ and $\vec{r}_{t+\Delta t}(p)$ are respectively the velocity and position of this site at the time $t+\Delta t$. In this way, next velocity and position of each site can be predicted, so that the trajectories and velocities of all sites can be predicted. Or in other words, the behavior of the system during a mechanical process can be predicted.

Wear of a material

As described earlier, if $\Delta l / l_0 > \varepsilon_y$, plastic deformation takes place, which produces irreversible strain when the force on the bond is removed. The residual strain can be expressed as: $\Delta\varepsilon_p = \Delta l / l_o - \varepsilon_y$. As a result, the length of the stress-free bond, l_0 will changes to $l_0' = l_0(1+\Delta\varepsilon_p)$. If a bond experiences a number of plastic deformation and the accumulated plastic deformation reaches the critical value for fracture, which corresponds to the fracture strain, the bond is broken.

If all of the bonds connecting a site or a cluster of sites are broken, the site or a cluster of sites will be worn away from the bulk material. Using this method, the loss of lattice sites can be predicted during a wear process.

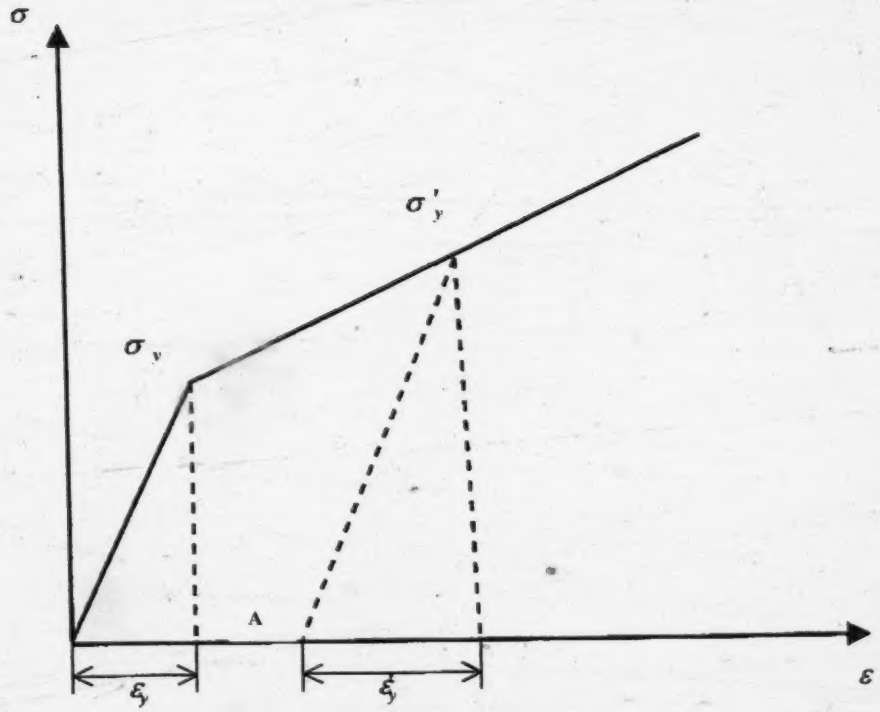

Fig.2.4 The schematic of stress-strain curve for work hardening

The work hardening of a material should also be taken into account. When the plastic deformation occurs, the yield strength (δ_y) and yield strain (ε_y) increases because of the work hardening. Fig.2.4 schematically illustrates the work hardening. Within the elastic region, the strain of a specimen will return to the original point after unloading. If the plastic deformation occurs, the stain will not return to the original point but to the point A after unloading. Hence the yield stain of material will change to ε'_y, which is larger than ε_y. Consequently, the yield strength δ_y increase to a higher value: δ'_y. The material is hardened with higher yield strength δ'_y.

2.3 The advantages and further development of MSDM

The main advantage of this model is that it is built based on a fundamental law i.e. Newton's law of motion: $\vec{F} = m \frac{d^2 \vec{r}}{dt^2}$. This equation is applied to wear with incorporation of the basic mechanical properties of materials. This makes it capable to predict the wear behavior of materials with different microstructures and to investigate the wear mechanisms. Since each site represents a cluster of atoms or a small volume of the material, the model can be used to simulate a wear process on micro- or macro-scales, so that both homogeneous and heterogeneous materials can be investigated. In addition, the model can simulate the wear process dynamically, which make it possible to predict wear in different modes, such as erosion, as a function of time and loading speed.

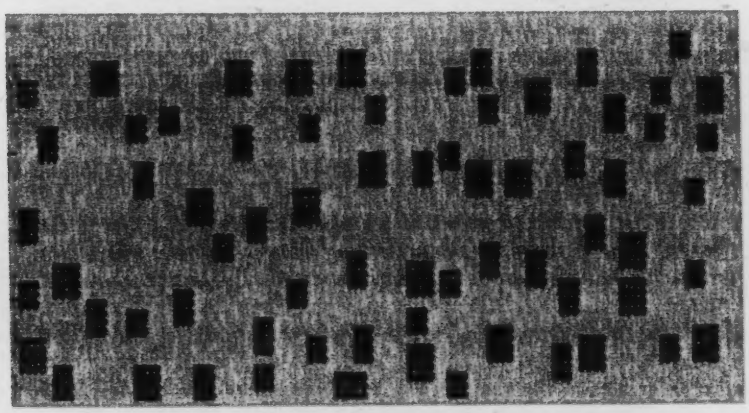

Fig.2.5 Schematic microstructure of 20%SiC-Al alloy

The model could be particularly useful for simulating wear of composites or multiphase materials, which are the main types of tribo materials. Fig.2.5 shows a

schematic microstructure of 20%SiC-Al alloy [35]. The MSDM can be used to investigate the effects of volume fraction, size, spatial distribution of the reinforcing particles on wear. The effects of interfacial bonding between the reinforcing phase and matrix on wear can also be studied if the interfacial bond strength is known.

Some factors, which influence the wear process, are not taken into account in the model. The most important factor is frictional heating. During a wear process, part of mechanical energy may change to thermal energy, thus raising surface temperature and consequently varying the properties of the material. Such variation, more or less, influences the accuracy of simulation, in which the mechanical properties of materials are assumed to be constant during wear. Fig.2.6 demonstrates the variation in erosive mass loss rate of 430 and 304 stainless steels with temperature. In the figure one may see that the wear rate is strongly influenced by temperature. The heat effect on wear process is very complex, which could induce phase transformations, soften a solid or even melt its surface [36]. Fig.2.7 shows the evidence of melting and re-solidification of aluminum on the surface of a silicon carbide particle that eroded an aluminum surface [37]. Incorporation of frictional heating into the MSDM would be planned for future development. Another factor affecting the accuracy of MSDM is the use of one "plastic modulus" to describe plastic

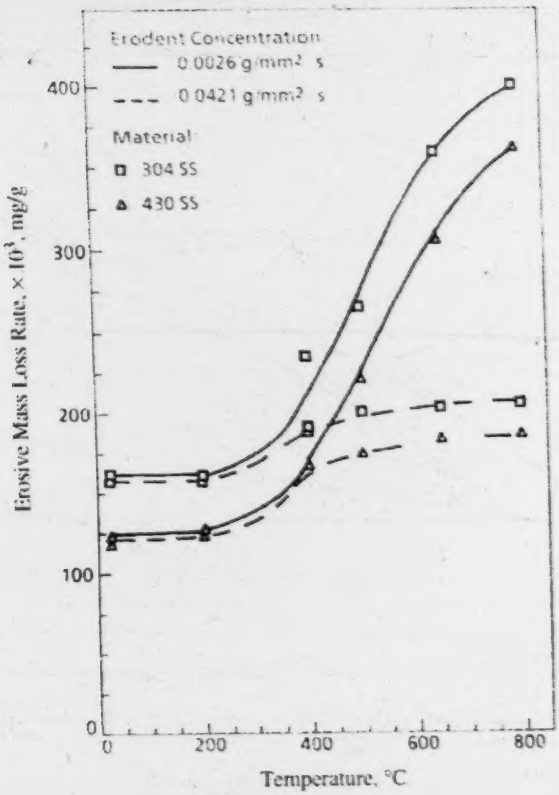

Fig. 2.6 Variation of erosive mass loss rate of 430 and 304 stainless steels with temperature for two erodent concentrations

behavior of a material. As shown in Fig.2.2, an approximate "plastic modulus" is to be constant and approximated using the slope of a line between the yield strength (σ_y) and the tensile strength (Ts) instead of using a nonlinear curve. In order to reduce the influence, the nonlinear curve can be simulated using a number of lines. Or in other words, we can use more than one "plastic modulus" (Ep) to reflect the plastic behavior.

Fig.2.7 Melted and resolidified aluminum on a silicon carbide erodent particle

2.4 Application of the MSDM in modeling erosive wear

The MSDM has been successfully applied to model abrasive wear. In this work, the MSDM was extended to simulation of solid-particle erosion of homogeneous and composite materials.

A solid-particle erosion process involves the interaction between the solid particles and a target material. Different from abrasive wear, the movement of sand particles needs to be modeled, which varies with time and affects the interaction between the target surface and sand particles.

Sand and target material need to be taken into account, which makes the model more complicated. To begin with, a simple system containing one sand and homogenous materials is considered here.

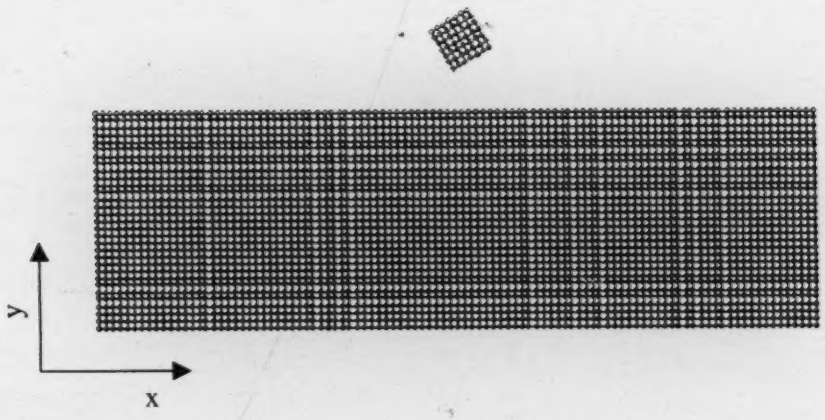

Fig.2.8 The sketch of the MSDM model for solid particle erosion

Fig.2.8 is a sketch of an erosion system, in which a sand particle and target material is descrtized and mapped using discrete lattices (square grid). Each site is connected to its adjacent sites by bonds. The unit length of the bond in the stress-free state is l_0.

The initial velocity of a sand particle is V_s along the direction with an angle of θ relative to the target surface. So the initial velocities of the sand particle in x direction and y direction are:

$$V_{sx} = V_s \cdot \sin(\theta) \tag{2.13}$$

$$V_{sy} = V_s \cdot \cos(\theta) \tag{2.14}$$

Before the distance between any two sites respectively on the surfaces of the target material and the sand is smaller than l_0, there is no interaction between the target and

sand materials. Velocities of all material sites are initially set to be zero. When a sand particle approaches the target material, interaction occurs and the following erosion process is governed by the Newton's law of motion as described earlier.

For a homogenous material, as described earlier, the site-site interaction may be expressed as:

$$f = k \cdot \Delta l \tag{2.15}$$

For a composite material, the reinforcing ceramic phase (only has elastic deformation) and the metal matrix (has both elastic and plastic deformations) will experience different deformations due to their different mechanical properties, as Fig.2.9 illustrates. The difference in the mechanical behavior makes the deformation of a bond between reinforcing phase and metal matrix complicated. The following is a list of various parameters in the model.

$l_\circ$	The unit length of the lattice or the bond length in stress-free state
l	Bond length after deformation
E	The slope of the stress-strain curve of a material
f	Force between a pair of adjacent sites
$f_{(c,m)}$	The force on the reinforcing phase site from the matrix site
$f_{(m,c)}$	The force on matrix site from the reinforcing phase site
Δl	Total deformation of a bond
Δlc	Deformation of the bond of reinforcing phase
Δl_m	Deformation of the matrix bond
Δl_{my}	Deformation of matrix bond at yielding
Ec	Elastic modules of reinforcing phase
E_{me}	Elastic modulus of matrix
E_{mp}	Plastic modulus of matrix
ε_y	Yield strain of matrix
ε_c	Strain of reinforcing phase
ε_m	Strain of matrix

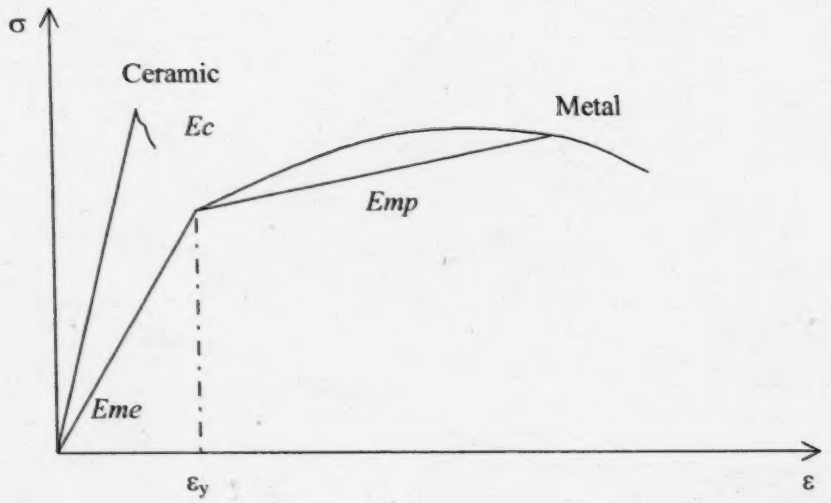

Fig.2.9 Schematic illustration of tensile curves of ceramic and metal material

1) When only elastic deformation occurs

$$\Delta l = \Delta l_c + \Delta l_m$$

$$\because f_{(c,m)} = Ec\,\varepsilon c l_\circ^2 = Ec\frac{\Delta lc}{\left(\frac{l_\circ}{2}\right)} l_\circ^2 = f_{(m,c)} = E_{me}\frac{\Delta l_m}{\left(\frac{l_\circ}{2}\right)} l_\circ^2 = E_{me}\varepsilon_m$$

$$\therefore \Delta l_m = \frac{Ec}{E_{me}}\Delta lc$$

$$\because \Delta l = \Delta lc + \Delta l_m = \Delta lc + \frac{Ec}{E_{me}}\Delta lc = (1 + \frac{Ec}{E_{me}})\Delta lc$$

$$\Delta lc = \frac{\Delta l}{1+\frac{Ec}{E_{me}}}, \qquad \Delta l_m = \frac{\Delta l}{1+\frac{E_{me}}{Ec}}$$

$$\therefore f_{(c,m)} = Ec\frac{\Delta lc}{l_\circ/2}l^2{}_\circ = 2Ec\Delta lcl_\circ = Ec\frac{2\Delta l}{1+\frac{Ec}{E_{me}}}l_\circ = \frac{2E_{me}Ec}{E_{me}+Ec}l_\circ\Delta l \qquad (2.16)$$

$$f_{(c,m)} = f_{(m,c)} \text{ (in opposite directions)}$$

Since Δl is dependent on the previous forces on the bond, the new force $f_{(c,m)}$ and $f_{(m,c)}$ can thus be calculated. Once $f_{(c,m)}$ and $f_{(m,c)}$ are obtained, one may predict next deformation. However, if ε_m is larger than ε_y, plastic deformation may occur. In this case, the force and deformation of a bond between reinforcing phase and matrix need to be calculated in another way:

2) When plastic deformation takes place

let $\delta l = \Delta l_m - \Delta l_{my}$, $\Delta l = \Delta l_c + \Delta l_m$

$$\because \quad f_{(m,c)} = E_{me}\frac{\Delta l_{my}}{\left(\frac{l_\circ}{2}\right)}l_\circ^2 + E_{mp}\frac{\delta l}{\left(\frac{l_\circ}{2}\right)}l_\circ^2 = f_{(c,m)} = E_c\frac{\Delta lc}{\left(\frac{l_\circ}{2}\right)}l_\circ^2$$

$$\therefore \quad E_{me}.\Delta l_y + E_{mp}(\Delta l - \Delta l_c - \Delta l_{my}) = Ec\Delta l_c$$

$$\Delta lc = \frac{E_{mp}\Delta l + (E_{me}-E_{mp})\Delta l_{my}}{(E_{mp}+Ec)} = \frac{\Delta l - (1-\frac{E_{me}}{E_{mp}})\Delta l_{my}}{(1+\frac{Ec}{E_{mp}})}$$

and

$$\Delta l_m = \Delta l - \Delta l_c = \Delta l_c \frac{Ec}{Emp} + (1 - \frac{Eme}{Emp})\Delta lmy$$

$$f_{(c,m)} = Ec \frac{\Delta lc}{\left(\frac{l_o}{2}\right)} l^2{}_o = 2Ec\Delta lcl_o = 2Ec \frac{\Delta l - (1 - \frac{E_{me}}{E_{mp}})\Delta l_{my}}{\left(1 + \frac{Ec}{E_{mp}}\right)} l_o = f_{(m,c)} \qquad (2.17)$$

Since the force on the site from adjacent sites is determined, the total force on a surface site, e.g., site p, is given by:

$$\vec{F}_p = \sum_1^n k \cdot \Delta \vec{l}\,(p, n) + \vec{f}_p \qquad (2.18)$$

where, $\vec{f}_p$ is an external force resulting from the impact of erodent, and n is the number of sites adjacent to this site. When the total force on the site is known at the time t, its velocity and position after a time interval Δt are determined by equations 2.10 and 2.11.

In such a way, the trajectory and position of each lattice site could be predicted. When the length of a bond between two adjacent sites exceeds a critical value corresponding to the fracture strain, the bond fails. Erosion loss results consequently when all bonds connecting a site or a cluster of sites to it adjacent sites are broken. Using this method, a dynamic process of solid-particle erosion could be simulated.

In the model, the number of total loss of sites was treated as erosion loss of target material. After the impact of each site, the target material was turned over and all of the broken sites should drop away from the surface of the target material due to gravity. With this method, the erosion loss of the target material can be calculated.

The accuracy of modeling is strongly influenced by the time interval, Δt. If Δt is too large, the deformation of a site-site bond, $\Delta l = V \cdot \Delta t$, could exceed the fracture strain of the material, thus resulting in a high erosion rate which is incorrect. However, one may

judge whether or not a proper Δt is selected, if plotting the erosion loss as a function of Δt, as illustrated in Fig.2.10. As shown, the erosion loss rapidly rises when Δt approaches 4.0E-6. Because the force $\bar{f} = k \cdot \Delta l$ and Δl is related to Δt, if Δt is too large, a large Δl will be generated that makes the bond broken suddenly, resulting in larger wear loss. Therefore, Δt should be smaller than this critical value. On the other hand, the selected Δt should not be too far away from the critical value in order to save computing time. Selection of Δt is actually influenced by the length of the stress-free site-site bond, $l_\circ$. The quantitative relationship between Δt and $l_\circ$ is under study.

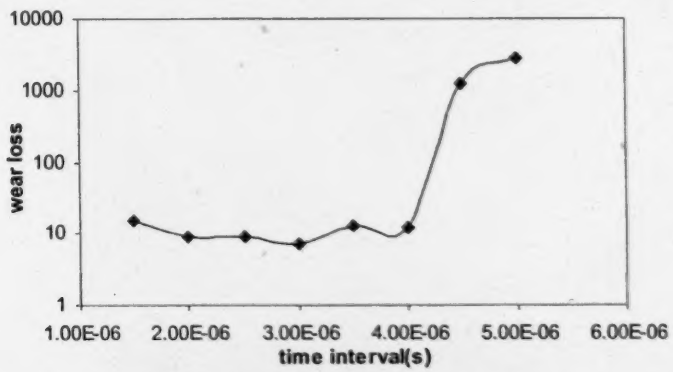

Fig.2.10 The influence of Δt on the wear loss

The parameters in equations 2.15-2.18 are all vectors. For two-dimensional modeling, each vector can be decomposed into two components respectively parallel to x and y directions. For three-dimensional modeling, a vector should be decomposed into three components parallel to x, y and z directions, respectively. 3D model may reveal a real wear process more accurately but take too much time to obtain results. Many papers have demonstrated that 2D modeling is sufficient to provide useful information on erosion [18-21].

In the present model, wear/erosion occurs when the site-site bonds are broken. A site or a cluster of sites is worn away when all bonds connecting it to its adjacent sites are broken.

In this model, the temperature effect is neglected. During solid-particle erosion, the temperature rise may not be large, since the heat generated during the process may be removed quickly by the sand flow with air. In the present work, the emphasis is put on studies of the effects of the microstructure and erosion condition on surface damage.

2.5 Summary

A promising method, the micro-scale dynamic model (MSDM), is described in this chapter. Compared to other models, the MSDM has many advantages. The model is built on Newton's law of motion and the erosion behavior of a material depends only on the fundamental mechanical properties of the material, such as Young's modulus, yield strength, tensile strength and the fracture strain. In contrast with macro-models and atomistic models, the MSDM can be used to investigate microstructural effects on wear and thus to provide guidelines for material selection and design.

In this study, the MSDM is applied to model erosion processes of homogeneous and heterogeneous materials and to investigate the effects of microstructure and erosion condition on surface failure.

Chapter 3

Simulation of solid-particle erosion processes for homogenous materials

3.1 Simulation Procedure

As discussed in chapter 1, it is difficult to investigate the mechanism of solid-particle erosion from experiment due to its complexity. Previous efforts were made to develop models to study this process. However, these models have various disadvantage and limitations. For example, it is difficult to use the models to investigate the influence of microstructure on wear and to predict the direction of crack propagation, which are important to investigate the mechanism of solid-particle erosion. In this work, the MSDM was applied to simulate this complex process. Silicon carbide and pure copper were selected as the target materials, and silicon carbide was also used as the erodent. In addition, processes of cracking in a brittle material under different conditions were also modeled and an artificial erodent was used in these processes. The materials were assumed to be homogeneous, whose mechanical properties are given in Table.3.1.

Table 3.1 Mechanical properties of materials under study [38]

Material	Modulus $E_e(GPa)$	Yield stress $\sigma_y(MPa)$	Tensile strength $\sigma_T(MPa)$	Fracture strain $\varepsilon_f(\%)$
Copper	110	69	200	45
SiC	430	862	862	0.2
Artificial erodent	1000	3448	3448	0.2

Two-dimensional modeling was performed to investigate erosion of the target materials and effects of the speed, shape and impact angle of the erodent particles on erosion. The length of a stress-free bond between two adjacent sites is set as 3×10^{-5} m,

the time step was chosen as $\Delta t = 3 \times 10^{-7}$ s. The target material and an erodent particle were discretized and mapped onto a lattice consisting of 100×80 and 7×7 sites, respectively.

3.2 Simulation Results

3.2.1 Effect of the erodent velocity on erosion

It is known that erosion is strongly affected by the erodent velocity. The effect of erodent velocity on erosion was predicted using the MSDM. In the present modeling, the erodent particles had a square shape and were ejected onto the target surface at an angle of 45 degrees. Figs. 3.1 and 3.2 illustrate the influences of the erodent velocity on the relative erosion losses of copper and SiC, typical metallic and ceramic materials, respectively. As demonstrated, with an increase in the erodent velocity, the erosion losses of both the target materials increased. The higher the erodent velocity, the larger were their erosion losses. For the ductile (Cu) and brittle (SiC) materials, the logarithmic relationship between the erosion loss and the impact velocity was approximately linear for tested velocity range. Such a relationship is

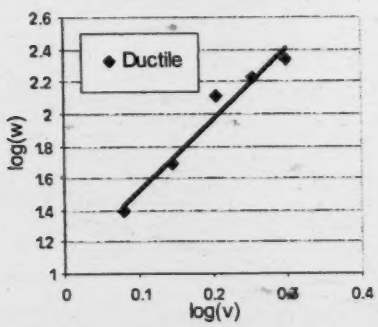

Fig.3.1 The influence of impact velocity on the erosion loss (ductile)

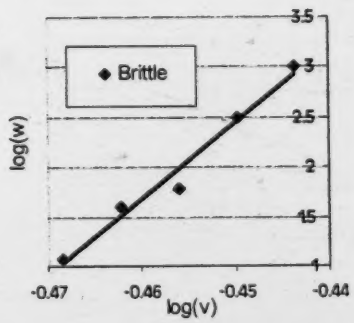

Fig.3.2 The influence of impact velocity on the erosion loss (ceramic)

consistent with previous studies, which demonstrate that the relation between the erosion loss (W) and the velocity (V) is expressed by the following equation:

$$W \propto V^n \quad \text{or} \quad \log W \propto n \log V \tag{1}$$

where n is a constant[39]. Hence the logarithmic relation between the erosion loss and the erodent velocity is linear, as Fig 3.1 and Fig 3.2 illustrate. Since in the model the erosion loss is represented by the number of sites worn out from surface, the figures only represent relative values rather than absolute ones. It needs to point out that the constant n may vary in different ranges of the erodent velocity [39].

3.2.2 Variations in erosion loss with respect to the impact angle

The relative erosion loss with respect to the impact angle for the brittle and ductile materials was studied and results are presented in Fig.3.3 and Fig.3.4, respectively. Fig.3.3 illustrates variations in erosion of copper against the impact angle. The maximum

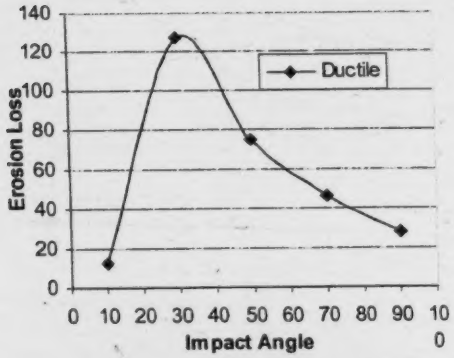

Fig.3.3 The relationship between the impact angle and the erosion loss (ductile material)

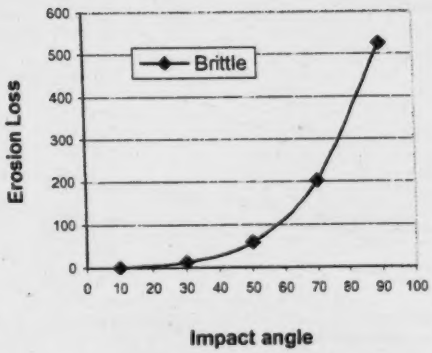

Fig.3.4 The relationship between the impact angle and the erosion loss (brittle material)

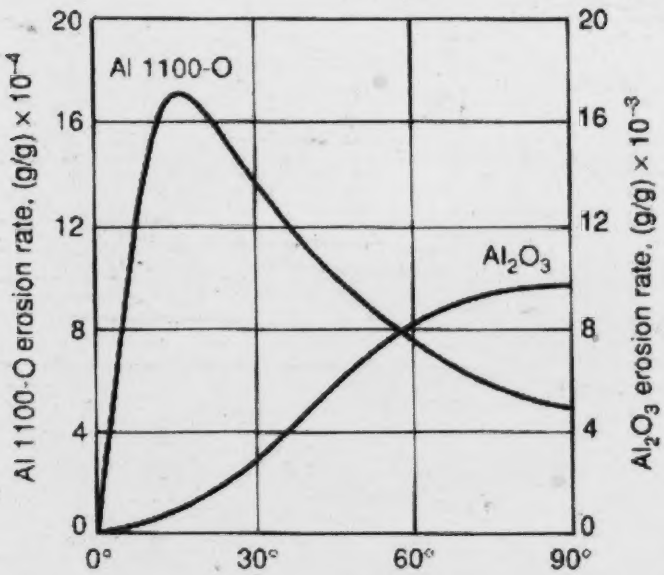

Fig.3.5 Erosion of 1100-O aluminum relative to Al_2O_3 both impinged by SiC particles

erosion occurred around 30°. While in the case of the brittle material (as show in Fig.3.4.), the maximum wear occurred at 90°. The simulation is consistent with experimental observation [39] (as Fig.3.5 showed).

In order to better understand the effect of impact angle on erosion, a close look was taken at the lattice distortion and damage of both the ductile and brittle target materials eroded respectively at impact angles of 30° and 90°. Fig.3.6 (a) and (b) and Fig.3.7 (a) and (b) illustrate the target materials after erosion at these two impact angles, respectively. For the ductile material, the damage to its lattice caused by impact at 30° was markedly larger than that caused by impact at 90°. Under the impact at 90°, the erosion loss was smaller, although the surface roughness increased due to the vertical impact of erodent particles. The situation was reversed in the case of erosion of the brittle target material. Cracking and damage of surface layer caused by impact at 90° were obviously enhanced, compared with those caused by impact at 30°.

(a)

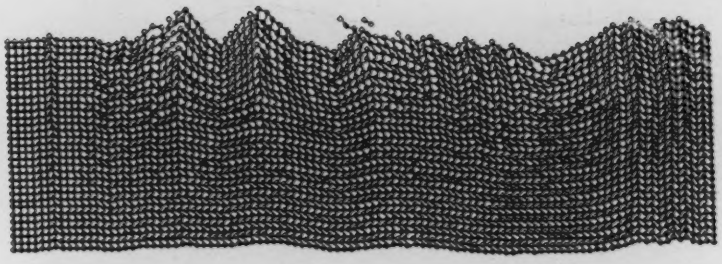

(b)

Fig.3.6 The surface morphology of ductile material after the impact by 30 erodent particles (a) impact angle = 30^0 and (b) impact angle = 90^0

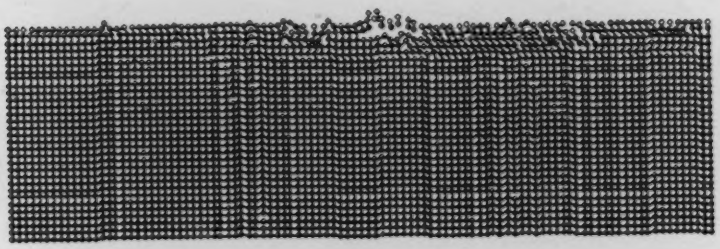

(a)

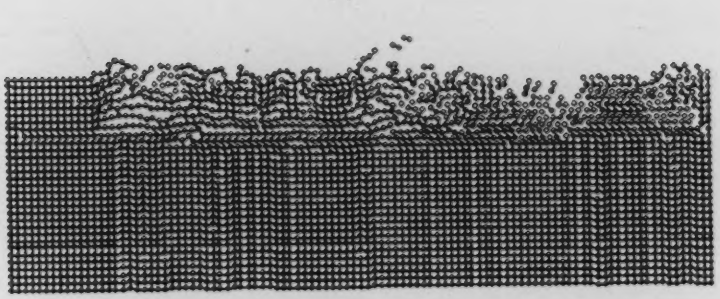

(b)

Fig.3.7 The surface morphology of brittle material after impact by 20 erodent particles

(a) impact angle = 30^0 and (b) impact angle = 90^0

The above phenomena are understandable. For a ductile material, it has a relatively high resistance to impact due to its good capability to accommodate plastic deformation. It is known that the fracture is generally caused by tensile or shear stress. If the target material is impinged by solid particles at 30°, the surface morphology of the target material is largely changed under the impact and it is easy for the erodent particles to interact with surface layer in lateral direction, which generates a lot of shear or tensile force on the surface layer and damage is easy to be generated. When impinged by solid particles at 90° (vertical direction), the lateral tensile stress may not affectively result in fracture due to the large fracture strain of the ductile material. As a result, a ductile material should have less damage when impacted at 90°. For a brittle material, however, the situation changes. The low ductility of the brittle material makes it vulnerable to deformation. Even under a compressive stress, the lateral expansion could be sufficient to cause fracture. Therefore, a brittle material is more sensitive to the impact energy. The impact energy increases when the impact angle changes from 30° to 90°. Consequently, the erosion damage increases as the impact angle increases and reaches its maximum at 90°. The lattice distortion and fracture shown in Fig.3.6 and Fig.3.7 clearly supports the above-discussed mechanisms.

The present study has demonstrated that the MSDM provides a promising tool to gain an insight into the erosion processes of ductile and brittle materials.

3.2.3 Influences of the shape and rotation angle of the erodent particles on erosion

Erosion is strongly influenced by the shape of erodent particles. For the present simulation, each particle consisted of 169 sites and the region under erosion attack was discretized and mapped onto a lattice consisting of 200×100 sites with a fixed boundary. The impact angle of sand was set as 40 degrees relative to the horizontal direction. Fig.3.8 shows the influence of particle shape, including triangle, square and circle, on erosion under the condition of single impact of an erodent particle. As demonstrated, the triangular particle resulted in the largest erosion loss, followed by the circular and square particles.

Such an effect of particle shape on erosion is understandable. For a triangular erodent particle, it had the smallest contact area and thus led to the largest contact stress and consequently the largest erosion loss. When impact at 40° without rotation, the square particle had the largest contact area. However, although it introduced the lowest contact stress, the square particle had stronger plowing effect than a circular-shaped particle had. As a result, the square particle resulted in the erosion loss on a similar level as that caused by the circular particle. However, if the square particle was rotated, larger wear could result. Fig.3.9 illustrates the effect of rotating erodent on wear. It was demonstrated that when the particle was rotated with a certain angle, the erosion loss increased. The phenomenon may be explained based on the contact area and consequent contact stress. As shown in Fig.3.9, 45-degree rotation resulted in the smallest contact area, so that the contact stress was the highest among the contact stresses caused by the

sand particles with the three rotation angles. Consequently, the 45 degree rotated sand caused the largest erosion loss.

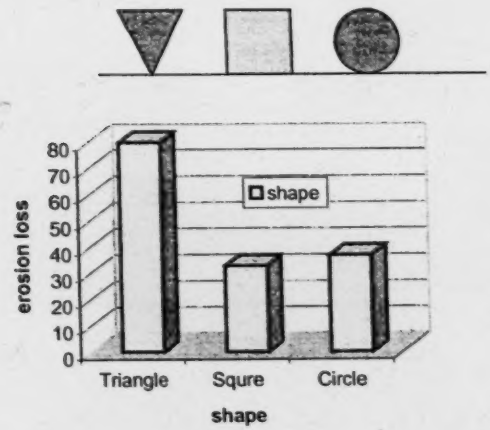

Fig.3.8 Influence of the erodent shape on the erosion loss of ductile material under the impact of one sand particle

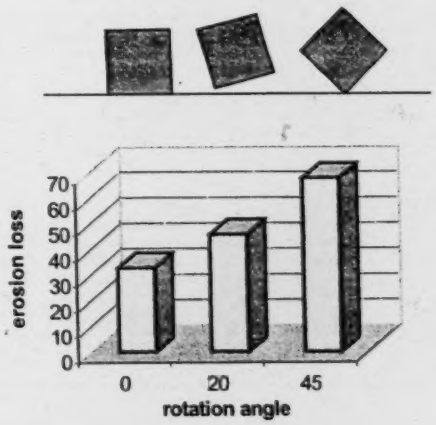

Fig.3.9 Erosion losses of the ductile materials under the impact of one sand particle with different rotation angles

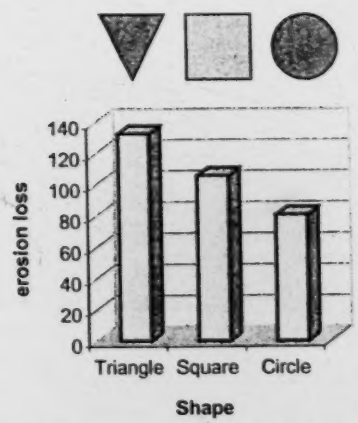

Fig.3.10 Influence of the erodent shape on the erosion loss of ductile material under the impact of 50 erodent particles

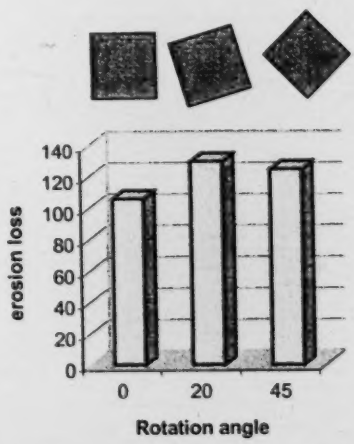

Fig.3.11 Erosion losses of the ductile material under the impact of 50 erodent particles with different rotation angles

In reality, erosion of a surface results from multi-impact by many particles rather than by a single particle impingement or single impact. Under multiple impacts, the result was different from that of single impact. As Fig.3.10 demonstrates, under multi-impact, the erosion loss caused by the square sand is larger than that caused by the circular sand. Such difference in erosion between single impact and multi-impact is understandable. After the impact by first erodent particle, plastic deformation was generated in the target surface layer. The deformation had two influences on the erosion process. First, the surface roughness increased because of material deformation, resulting in enhanced abrasive plowing. Secondly, the orientation between the local target surface and the surface of a square particle would change from zero to a certain degree, which enhanced surface cutting and plowing. For circular sand, the increase in surface roughness also made the surface easier to be plowed. However, lower contact stress caused by the circular erodent particles reduced the erosion loss, compared with those caused by angular erodent particles.

In order to better understand the erosion process, the erosion losses caused by multi-impact (by 50 square particles) as a function of the rotation angle was studied. Fig 3.11 illustrates the influence of the rotation angle on the erosion loss under multi-impact condition. Under the multi-impact condition, the rotation angle made a much smaller difference in erosion loss. As mentioned earlier, the surface roughness has a great influence on erosion. Under multi-impact, the target surface became rougher, which changed the local contact between the erodent particles and the target surface. Statistically, this may reduce the difference in erosion loss caused by particles with

different rotation angles, thus resulting in closer erosion losses. Results of the simulation are consistent with experimental observations [39].

3.2.4 Crack propagation in brittle material

The erosion loss of a brittle material during solid-particle erosion mainly results from fracture or cracking. It is of importance to investigate the failure process for understanding the erosion of brittle materials and the mechanism involved. In this study, the erosion of SiC caused by triangle erodent particles with their front angle respectively equal to 45, 90 and 135 degrees was investigated. The erodent particles were ejected along the vertical direction to the target surface. The propagation of horizontal and vertical crack was observed as illustrated in Fig.3.12. For a sharp erodent particle with 45-degree angle, the crack propagating in the vertical direction was much quicker than that in the horizontal direction. For an erodent particle with a larger angle, horizontal cracking was enhanced, due to the increase in tensile stress

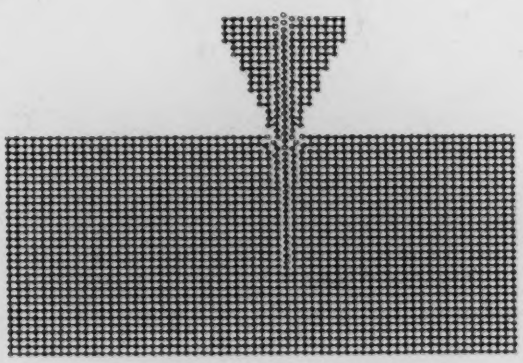

a)

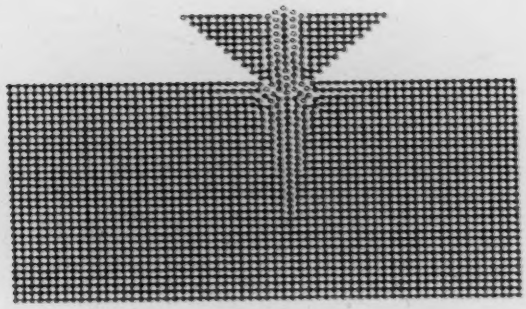

b)

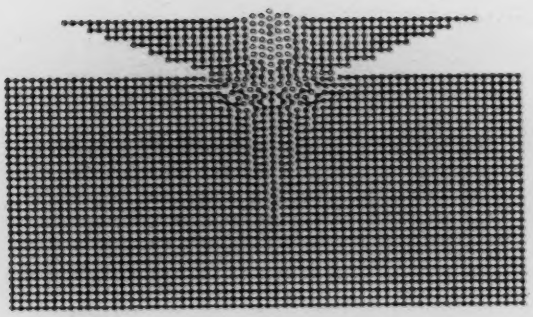

c)

Fig.3.12 Simulation of crack propagation in the brittle material (The artificial erodent was used here).

a) angle: 45^0 b) angle: 90^0 c) angle: 135^0.

component in the horizontal direction. The impact by the triangular particle, whose front angle was equal to 135^0 was similar to the impact by a spherical particle. Under the

impact of a spherical particle, there would be three kinds of cracks. Radial cracks are first formed, which spread outward from the periphery of the crack; with an increase in load, propagation of the cracks that are symmetric about the load axis will be enhanced in the subsurface; finally these cracks will merge with the radial cracks and grow into lateral cracks which propagate approximately parallel to the surface [40]. Fig.3.13 schematically illustrates the crack propagation under the impact of a spherical particle, where the lateral cracks are the main cracks, which propagate approximately parallel to the surface. The propagation of the median cracks that are vertical to the surface could be inhibited. A similar trend occurred in the present simulation of the impact by a large-angle erodent particle, as illustrated in Fig.3.12(c). However, because of the angular tip of the triangle particle, it tore the material, thus retaining the crack propagation vertical to the surface. With an increase in the tip sharpness, propagation of the median cracks that are vertical to the surface will be inhibited. Similar trend was observed in the present simulation of the impact by a large-angle erodent particle, as illustrated in Fig.3.12(c). However, because of the angular tip of the triangular particle, the main crack propagation was still vertical to the surface with enhanced lateral cracking. As the tip sharpness was increased, the median vertical crack propagation was further enhanced, as described by P. Ostojic [41](see Fig 3.14). In this case, lateral cracking will be inhibited by near-surface compressive stress. Such a phenomenon is well reflected by the present modeling of impact by a sharp triangular particle as illustrated in Fig.3.12 (a). Fig.3.12 (b) represents the situation of impact by a less sharp particle. In this case, both lateral and median vertical cracks could propagate. When cracks extended to the target surface, material delamination occurred.

Fig 3.13 Schematic illustration of crack growth under a spherical particle

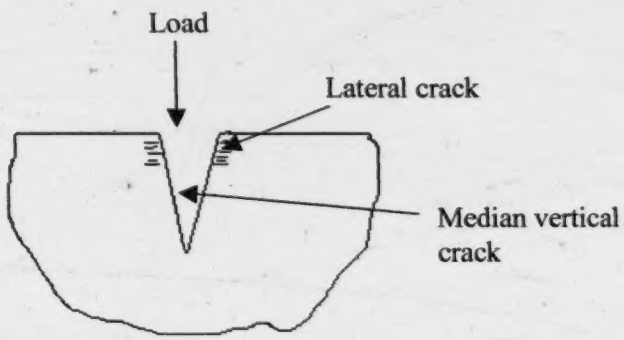

Fig 3.14 Schematic illustration of crack growth under a sharp tip

3.3 Conclusion

A dynamic model was developed based on a MSDM technique. This chapter reports the application of the model in simulation of solid-particle erosion of homogenous materials. In this model, the target material and solid particles are discretized and mapped

using discrete lattices, each site of which represents a small volume of the materials. Under external impact force, each site may move and its velocity and position are determined by Newton's law of motion. Erosion of typical ductile and brittle materials, copper and silicon carbide, were modeled. Erosion of the materials is dependent on their basic mechanical properties, including elastic modulus, yield stress, tensile strength, and ductility. No empirical equation is included in the model, so that the model is effective for prediction of erosion behavior of materials. The influences of impact angle, impact velocity, shape, and rotation angle of the erodent particles on the erosion process were investigated. Cracking in the brittle material under erodent particle impact was also studied. It was demonstrated that this model well reflected the relationship between these factors and the erosion loss and simulation results were consistent with experimental observations. The present study has demonstrated the efficiency of the MSDM in studying erosive wear. With further improvement of the model for more quantitative simulation, the MSDM would be developed into an effective computational tool for exploring erosion processes and elucidating the erosion mechanisms involved.

Chapter 4

Simulation of a solid-particle erosion process for composite materials

4.1 Introduction

Metal-matrix composites are often used as erosion-resistant materials due to their superior wear resistance [42]. In order to improve the performance of the composites, it is important to understand the mechanism responsible for solid-particle erosion of composite materials. For a composite material, its surface damage by solid-particle erosion depends on many factors, including the impact velocity, particle size and shape of the erodent, mechanical properties of both the target material and the erodent, and the volume fraction, size and properties of the reinforcing phase as well as the bonding between the matrix and the reinforcing phase. The synergism of these factors makes it difficult to experimentally investigate the erosion mechanism for composite materials. Computer simulation provides an effective and economic approach for such investigation.

As demonstrated in chapter 3, the MSDM has been applied to simulate a homogenous material successfully and the simulation results were consistent with observations. In order to investigate the effect of microstructure on solid-particle erosion, the model was further developed by taking account of reinforcing phases in a homogenous material. The reinforcing phases have great influence on erosion process. The bond strength between a reinforcing phase and the matrix is also an important factor affecting the erosion resistance of composite. In this work, microstructural effects on erosion of composites were investigated using the MSDM. The studies demonstrate the effectiveness of the computer model for erosion prediction and fundamental investigation of erosion mechanisms and its potential applications in material design. In this work, copper and silicon carbide were selected as the matrix material and reinforcing phase,

respectively. In addition, silicon carbide was also used as the erodent. Mechanical properties of the materials have been given in Table 3.1.

Two-dimensional modeling was performed to simulate erosion process. The length of a stress-free site-site bond between two adjacent sites was set as 3×10^{-5} m, the time step was chosen as $\Delta t = 3\times10^{-6}$ s. The target material was discretized and mapped onto a lattice consisting of 120×80 sites. In order to simplify the simulation, only

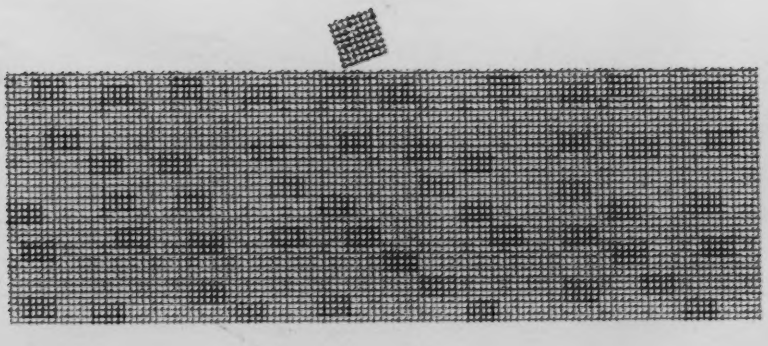

Fig.4.1 The sketch of solid-particle erosion of a composite material

rectangle reinforcing particles were randomly embedded in the matrix, as illustrated in Fig.4.1. In addition, the bond between the matrix and reinforcing phase was assumed to be an elastic bond. The details about how to calculate the interaction between a reinforcing phase site and a matrix site have been described in chapter 2.

4.2 Results and discussion

4.2.1 Effect of the volume fraction of the reinforcing phase on erosion

The erosion resistance of a composite material is affected by the volume fraction of its reinforcing phase. The effect of the volume fraction of the reinforcing phase on erosion was first investigated. In this study, three different sizes of second-phase particles were used, which consisted of 4, 24 and 96 sites, respectively. The bond strength between the matrix and the reinforcing phase was set to be perfect, i.e. it is even much stronger than the bond strength of reinforcing phase. The erosion condition was the same for the three composites, i.e. the sand flow, sand size and shape were the same for the three composites. Fig.4.2 illustrates the predicted erosion losses against the volume fraction of the reinforcing phase with different particle sizes. As demonstrated, the erosion loss decreased initially with an increase in the volume fraction of the reinforcing phase. After reaching a minimum value, the erosion loss increased with an increase in the volume fraction of the reinforcing phase.

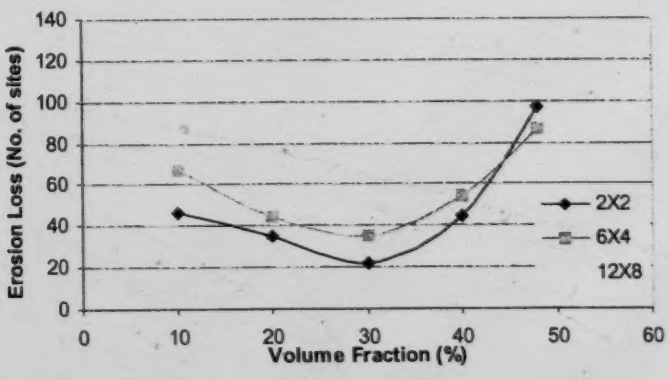

Fig.4.2 Erosion loss vs the volume fraction of the reinforcing phase having different particle sizes

The observed relationship between the erosion loss and the composite material is understandable. The relatively soft matrix was strengthened by the embedded reinforcing particles. The reinforcing phase made it difficult to remove the material from surface. On the other hand, the relatively brittle reinforcing phase was protected by the ductile matrix that absorbed the impact energy, accommodated large-scale deformation and bound the reinforcing phase. These factors all affected the erosion resistance of a composite material. With a small volume fraction of the reinforcing phase, the first factor may have greater influence on the reduction of erosion. However, when too much reinforcing phase was introduced, the composite became brittle. The loss of ductility or less protection of the reinforcing phase from the erodent impact led to an increase in the erosion loss. Such a phenomenon was observed during sliding wear of composite materials [43].

4.2.2 Effect of interfacial bonding on erosion

The bond strength of the interface between the matrix and the reinforcing phase has a great influence on the erosion resistance of composites. Computational studies were conducted to investigate this influence using the MSDM. Fig.4.3 illustrates the effect of the interfacial bond on the erosion of a composite that contained 20% reinforcing phase. In order to exclude the influence of other factors, three composites having the same matrix, same reinforcing phase but different bond strengths were studied. The composites were also under the same erosion condition (the same mass flow of erodent particles with the same impact velocity). Three bonds (weak, medium and strong) were considered. The

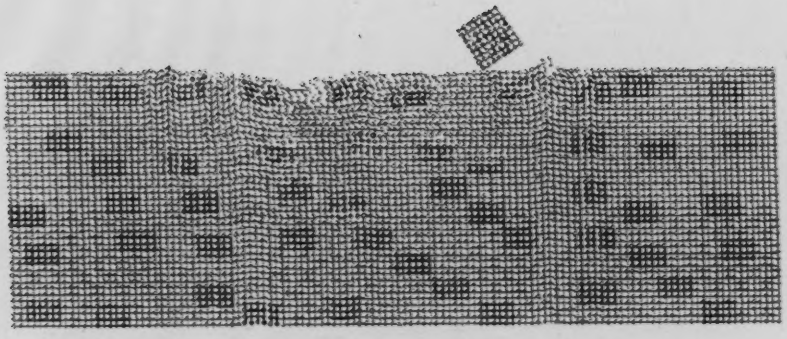

a) Strong bond

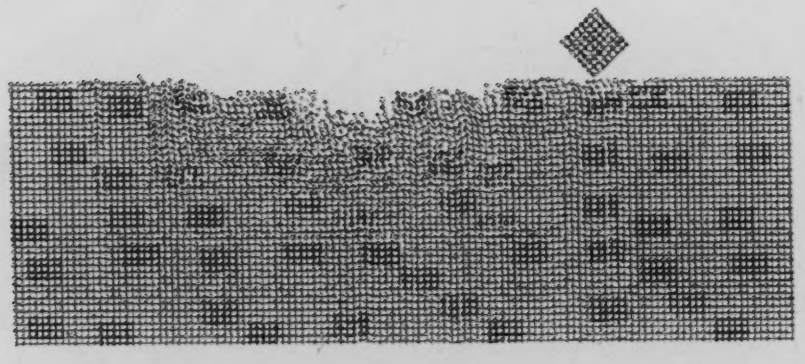

b) Medium bond

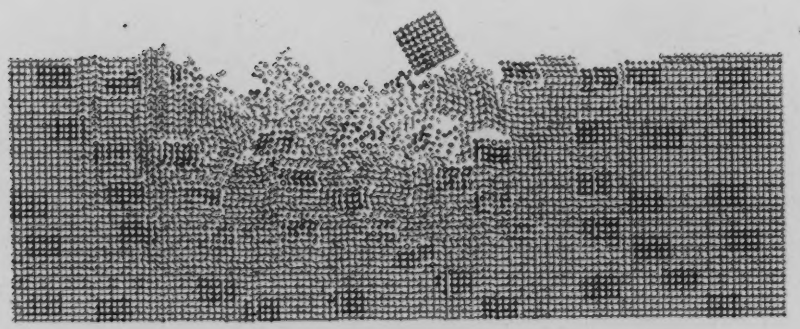

c) Weak bond

Fig.4.3 Solid-particle erosion of composites with strong, medium and weak interfacial bonds

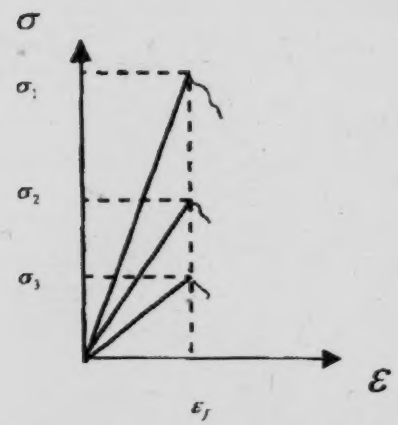

Fig.4.4 The strengths of three interfacial bonds: σ_1 ____ strong bond, σ_2 ____ medium bond, and σ_3 ___ weak bond

bond strength was determined by the maximum tensile stress under which the bond failed. As shown in Fig.4.4, the three bonds had the same fracture strain but different maximum tensile stresses at fracture. Here ε_f =0.002, σ_1 =800MPa, σ_2 =80MPa and σ_3 =8Mpa. The erosion damage increased considerably with a decrease in the bond strength. As expected, the weak bond was broken easily under the impact of erodent, thus resulting in cracking in the composite, associated with low erosion resistance.

Since the erosion resistance depends on the properties of both the materials (i.e. the reinforcing phase and the matrix) and the interfacial bond strength strongly affects the role of the reinforcing phase. Simulation was conducted to investigate how the interfacial bond affected the entire role of the reinforcing phase against erosion. Fig.4.5 illustrates the simulation result of the erosion loss as a function of the volume fraction with three different interfacial bonds. As demonstrated, with a decrease in the interfacial bond strength, the minimum erosion loss shifted to the left with lower volume fraction of the

reinforcing phase. For the weak bond, the erosion loss continuously increased with an increase in the volume fraction of the reinforcing phase.

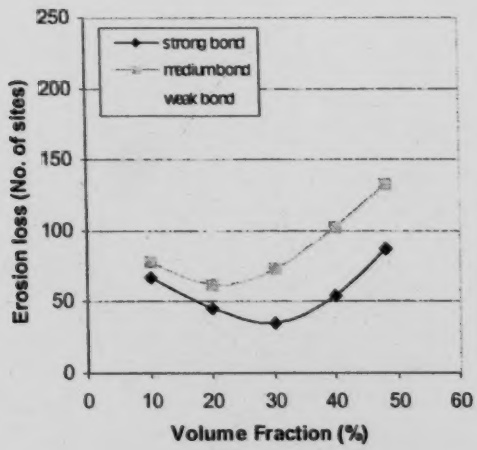

Fig.4.5 Erosion losses vs the volume fraction of the reinforcing phase for three different interfacial bonds

The simulation clearly indicates that when the interfacial bond is weak, the reinforcing phase is not functional, and instead, the interface become the preferable place for fracture to occur, thus leading to the decreased resistance to erosion. As the interfacial bond strength increased, the reinforcing phase became functional, and the minimum erosion loss or the maximum erosion resistance could be achieved at higher volume fractions of the reinforcing phase as Fig.4.5 illustrates.

4.2.3 Effect of the erodent size on erosion

The erosion process of a composite is influenced by the size of erodent. In this work, the erosion of a composite by erodent particles with three different sizes was simulated. The mass flow of erodent particles kept the same for all the three particle sizes. This means that the total mass of the erodent striking a target surface for each erosion process was the same. The erodent particles with three different sizes consisted of 144, 64 and 16 sites, respectively. Hence, the size ratio (or area ratio for 2D simulation) among the erodent particles having three different sizes was 9:4:1. In order to investigate erosion of a composite under the impact of differently sized erodent particles at the same mass flow, the ratio of the erodent-particle number for the three erodent sizes was set as 1:4:9.

Fig.4.6 illustrates the simulation results of erosion caused by erodent with different particle sizes. One may see that as the erodent size increased, the erosion damage to the target material increased. Such a trend is consistent with experimental observation [44]. This relationship between the erodent size and erosion loss is understandable. When an erodent particle was in contact with the target material's surface, the sharp edge of the particle struck the surface first. For an erodent particle with large size, it is easy for the particle to cut into the target material and plow its surface due to a large impact stress on the area exerted by the particle. Or in other words, a large impact force was exerted on a small area where the sharp edge of a particle was in

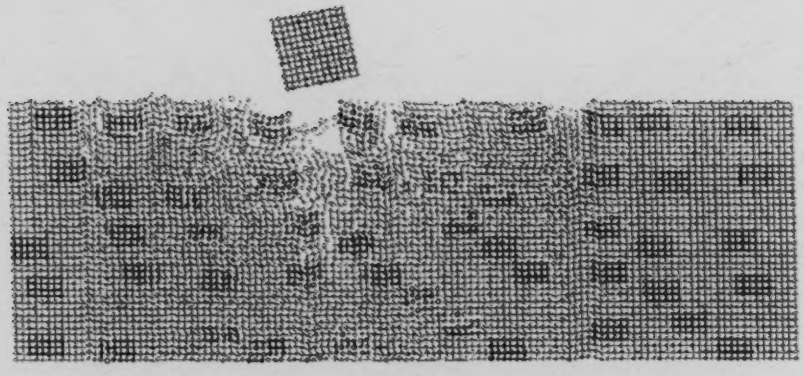

sand number = 10

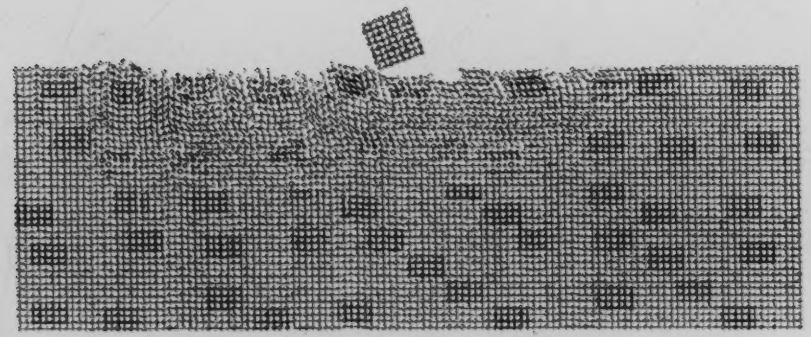

sand number = 40

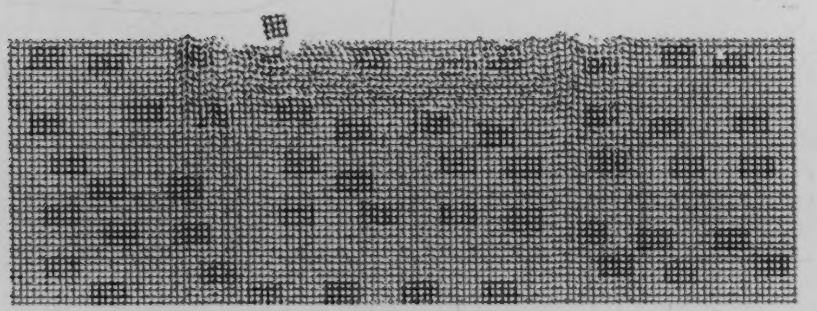

sand number = 90

Fig.4.6 Erosion of a composite caused by erodent respectively having three different particle sizes (under the same mass flow of the erodent)

contact with the target material, thus resulting in a large impact stress and consequently larger damage. In addition, cracks are also easy to be generated in the hard but brittle reinforcing phase because of the larger impact stress. However, for the erodent with a smaller particle size, the erosion decreased due to lower striking force, although the mass flow of the erodent was the same as that of the erodent with a larger particle size.

4.2.4 Effect of the size ratio of the erodent to the reinforcing phase on erosion

The ratio of the erodent particle size to that of the reinforcing phase also affected the erosion process of the composite material. Fig.4.7 illustrates the erosion of a composite containing 20% reinforcing particles having three sizes, respectively. The erodent particle size kept the same and the same mass flow of erodent particles was used for each case. In the study, each erodent particle was composed of 12X12 sites and the three different sizes of the reinforcing particles were12X8, 6X4 and 3X2, respectively. It was assumed that the interfacial bond strength was strong. The size ratios of the erodent to the reinforcing particles for the three composites were 3:2, 6:1 and 24:1, respectively.

As shown in Fig.7, the smallest size ratio (i.e. 3:2) resulted in the largest erosion damage, while the largest size ratio (24:1) led to the smallest erosion damage. The erosion damage was reduced with an increase in the size ratio. Such a trend is consistent with experiment observation reported in literature [44].

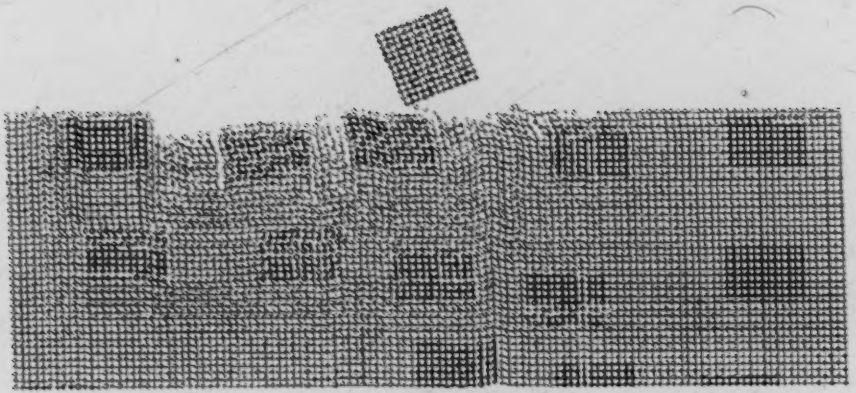

Size ratio = 3:2

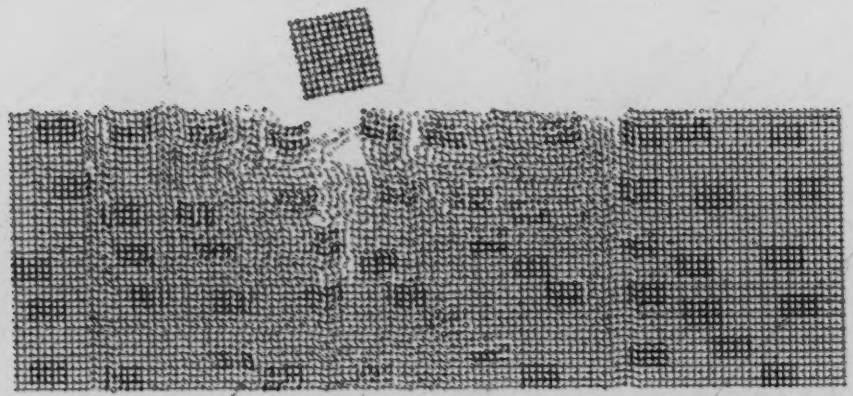

Size ratio = 6:1

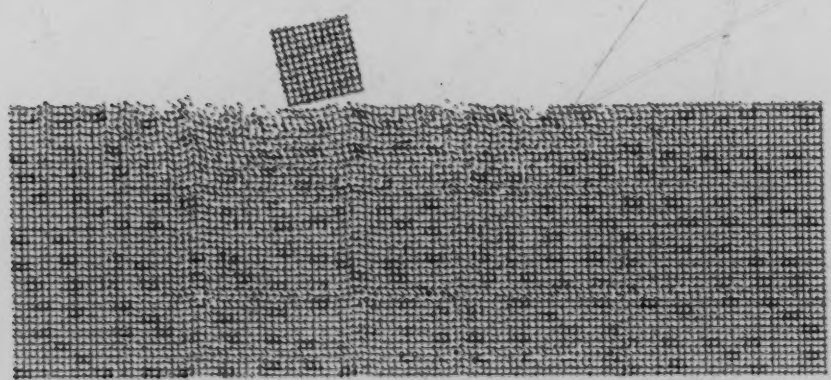

Size ratio = 24:1

Fig.4.7 Erosion of the composite for three size ratios (The volume fraction of the reinforcing phase was the same)

The observed phenomenon, i.e. the erosion loss decreased as the size ratio increased, could be explained. A composite having small reinforcing particles has higher erosion resistance than that having large reinforcing particles. This is expected because the small dispersed reinforcing particles are more protected due to the existence of more interfaces with smaller distance between the reinforcing particles. Such a microstructure is more effective to block the motion of dislocations. Furthermore, the finer hard but brittle reinforcing particles can also be protected effectively by the surrounding ductile matrix. If the size ratio is small, it is easier for erodent to strike the matrix and reinforcing phase separately. As a result, the ductile matrix is easier to be cut and plowed away from surface without the protection of the reinforcing phase. It is also easier for the reinforcing phase to be damaged under the direct impact of erodent with less protection by the ductile matrix.

4.3 Conclusion

A dynamic model based on the MSDM technique was applied to simulate solid-particle erosion of composite materials with the emphasis on the effect of microstructure on erosion damage. In this work, effects of the volume fraction of reinforcing phase, interfacial bonding and erodent size on erosion, as well as the relationship between the size ratio of the erodent to the reinforcing phase and erosion damage were investigated using the MSDM. It was demonstrated that the model was effective for investigating the mechanism responsible for erosion of materials and help to establish the relationship between the microstructure of a material and its behavior. The model allows visualizing

the erosion process. Such a capability would help us to obtain direct information on the failure mechanism in detail.

In addition to justification of the model, the following information on erosion was obtained, which is consistent with experimental observations or theoretical studies reported in literature.

1. With an increase in the volume fraction of reinforcing phase, the erosion loss of a composite decreased. However, the erosion loss increased if too much reinforcing phase was added.
2. The stronger the interfacial bond strength, the higher the erosion resistance. If the interfacial bond was weak, the reinforcing phase became harmful, since it increased the probability of cracking at the interface.
3. With a decrease in the interfacial bond strength, the minimum erosion loss shifted to a lower volume fraction of the reinforcing phase. For a weak bond, the erosion loss may continuously increase with an increase in the volume fraction of the reinforcing phase.
4. Under the same mass flow, more erosion loss was generated as the erodent particle size increased.
5. The ratio of the size of the erodent particle to that of the reinforcing particles had strong influence on erosion. The erosion loss decreased with an increase in the size ratio.

Chapter 5

Other Applications of the MSDM Technique

As demonstrated in chapter 3 and 4, the MSDM technique can be applied to investigate the erosion of materials and the influence of microstruture on erosion. It can also be used to analyze the crack propagation under the impact of particle with different geometries. Since the MSDM technique was developed based on a fundamental physical law, it could also be applied to study other types of wear and relevant phenomena. This chapter reports application of the model to investigation of interfacial failure and effect of nano paticles on wear of a pseudoelastic composite.

5.1 The application of MSDM in investigation of interfacial debonding

5.1.1 Introduction to an interfacial bonding test technique

Interfacial bonding is of importance to tribo-composite materials, thin films or coatings and multiphase alloys. This parameter determines the ultimate mechanical properties of the materials. Determination of interfacial bonding strength has been a subject of many investigations and attracted extensive attention from materials scientists and engineers.

There have been a number of methods proposed to evaluate interfacial bonding strength either for composites or for thin films and coatings [45-51]. However, none of them is "ideal" and many methods are qualitative in nature and only indicate whether an interface is "good" or "bad" [45]. In addition, their application is also limited due to (1) lack of transferability of measurement results, that is, the result obtained using one method is not consistent with those obtained using others. (2) lack of generality or not suitable for all different types of interfaces.(3) unjustified hypotheses or assumptions

used to build the methods. It is therefore necessary to develop an effective and general technique that can be used to quantitatively determine different types of interface.

Microindentation provides a promising method for evaluation of interfacial bond strength. There are a few possible ways to determine the interfacial bonding. The commonly used one is to perform indentation test on a coating surface to determine interfacial failure from the kinks on load-displacement curve [52,53]. This method may be suitable for the soft film or coating on the hard substrate [54], but not suitable for hard films due to the factor that the cracking of the hard film or coating can also result in kinks. In addition, the indentation performed on the coating surface makes analysis difficult. Furthermore, the method is not suitable for evaluating interfaces of composites in such a way. J.Bystrzycki et al. [55] and W.J.Fan et al. [56] performed cross-sectional indentation on substrate near a interface. They evaluate the interfacial bonding by determining the ratio of the crack length to the corresponding diagonal of the indent under a certain load. However, it is difficult to determine the initiation of debonding and the ratio can not be quantitatively related to the bonding strength. The indentation is also performed directly at the interface between the substrate and a coating [57,58]. However, cracking may occur inside the hard/brittle coating [58]. In addition, as above mentioned, the indentation is also used to push the fiber out to get the shear strength for fiber-matrix composites even some limitations are related.

Recently, a novel microindentation technique for determination of the interfacial bond was proposed [59]. To evaluate an interfacial bond, microindentation was performed near the interface (see Fig.5.1). Normal load~time and lateral force~time

curves were plotted simultaneously. It was noticed that the lateral force (Fx) was very sensitive to the debonding, therefore, the critical load could be obtained.

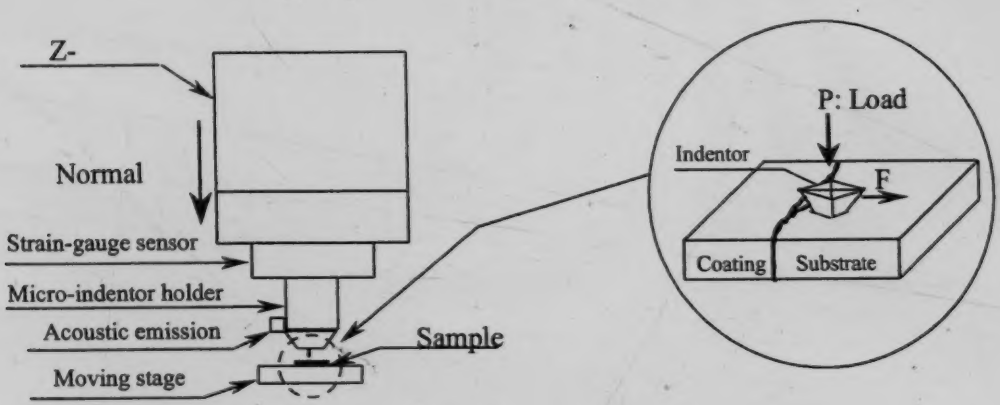

Fig.5.1 Schematic diagram of the indentation measurement

5.1.2 Experimental results

Fig.5.2 presents Fx – t and normal load – t curves for three Al_2O_3/Steel interfaces with different bond strengths. When the load was applied to the specimen having a weak interface (Fig.5.2 (a)), the interface failed under an intentation on load of 7N at which the slope of the Fx – t curve changed its sign. For the medium interface (Fig.5.2(b)), the slope of Fx – t curve changed its sign when the indentation load reached 30N. For the strong interfacial bond, no change in sign of the slope of Fx~t curve and no interfacial cracking were observed (see Fig.5.2 (c)). Therefore, it appears that the change in the sign of the slope of Fx~t curve is the point corresponding to the initiation of interfacial cracking and the corresponding normal load may be taken as the critical load that results in the interface debonding.

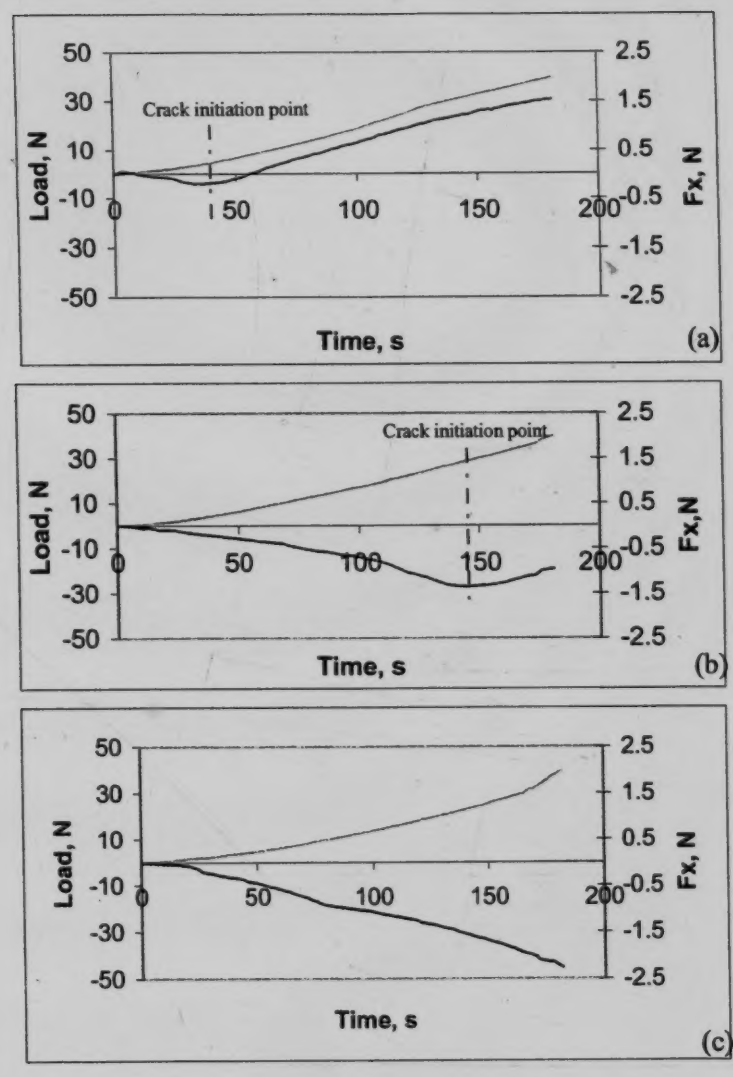

Fig.5.2 Curves of load-time and lateral-time for Al_2O_3/Steel bonding (a) weak bonding (b) strong bonding (c) very strong bonding

The correlation between the interfacial debonding and the change in sign of the slope of Fx – t curve could be explained in the following way. When indentation is performed on a homogeneous bulk material, the constraint of the specimen to the indenter should be the same along all radical directions and the lateral force is zero because of

cylindrical symmetry. However, when indentation is carried out near an interface, the constraint around the indentor is no longer symmetrical about a central line. As a result, the lateral force occurs. At the beginning of indentation, the larger constraint from the ceramic side leads to the indenter to move away from the interface. However, as the interfacial debonding occurs, the constraint from the ceramic side significantly decreased. As a result, the tip would move toward to the ceramic resulting in the change in sign of the slope of Fx~t curve. Therefore, it is possible to determine the critical load for the crack initiation from this change in sign of the slope of the Fx~t curve.

However, it is difficult to experimentally confirm this hypothesis regarding the correlation between the interfacial debonding and the change in the sign of the slope of the Fx – t curve. In order to justify the proposed correlation between interfacial debonding and the sign change of slope, the indentation process was simulated using the MSDM technique.

5.1.3 Modeling of interfacial debonding

In this model, again, a given specimen containing an interface is discretized using lattices as illustrated in Fig.5.3. Each lattice site represents a small volume of material. Under the influence of the interaction between the tip and the target surface, lattice sites may move and the total force on it determines its motion.

As shown in Fig.5.3, the target material is divided into two parts. The red part represents a ceramic phase and the blue part represents a ductile material. They are connected by

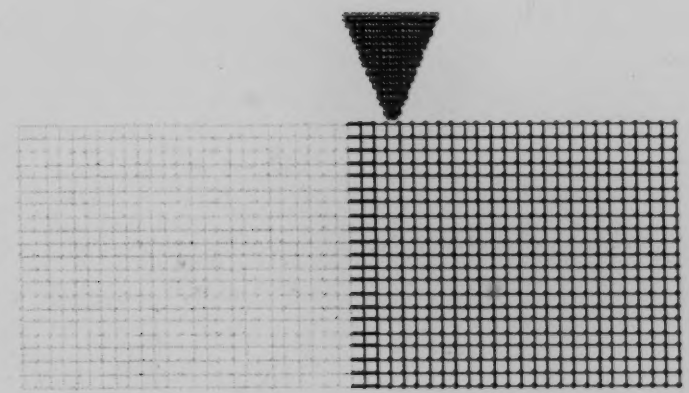

Fig.5.3 The target material and indenter are discretized

interfacial bonds (The black bond in the figure). The indenter is also descretized with a smaller scale.

The force coefficient of the ceramic bond is much larger than that of the ductile bond. The force coefficient of the interface bond is larger than that of the ductile bond but smaller than that of the ceramic bond. The interfacial bond is assumed to be elastic. In present simulation, in order to investigate the influence of the interface bond on indentation, three types of bonds were used, including a strong bond, whose strength was almost same as the ceramic bond, a medium bond, whose strength was between the ceramic bond and the metal bond, and a weak bond, whose strength was weaker than that of the ductile material. All the three types of bond were assumed to have the same critical length at fracture.

5.1.4 Analysis of simulation results

In the model, the displacement of indentor in the direction parallel to the surface was recorded against time. Fig.5.4 to Fig.5.7 present the simulation results for the three kinds of bond.

In the case of the strong interfacial bond, the lateral displacement increased with time, as Fig5.4 (b) illustrated. During indentation, the tip went down and penetrated into the target material under a normal load. The site-site bonds near the tip were compressed and deformed. Compared to the region on the right side of the tip, the region on the left side was harder to be compressed because of the hard phase that provides larger constraint to the tip. As a result, the tip moves toward the right-hand side because of the unsymmetrical constraint. Fig.5.4 (a) shows that the deformation of the interface bonds was small and little fracture occurred.

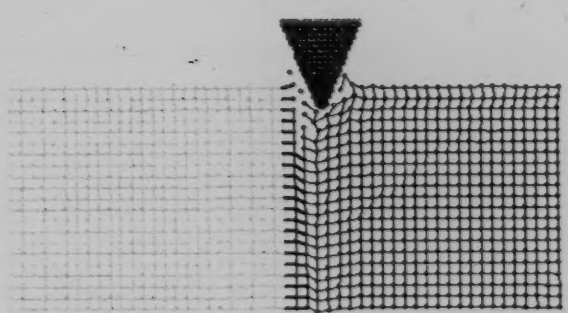

(a)

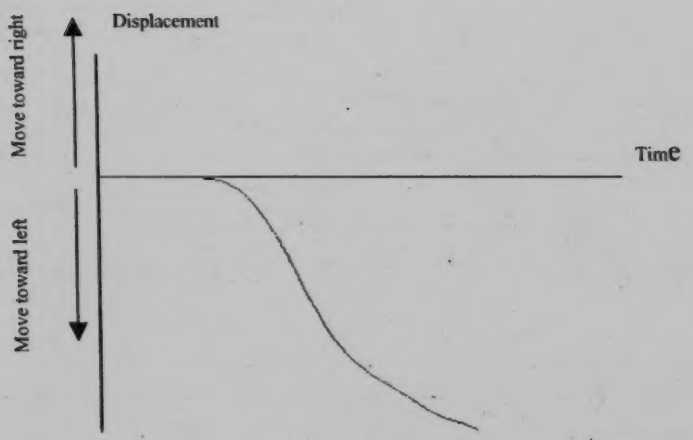

(b)

Fig.5.4 The simulation results for the strong interface bond. (a) Final simulation figure of indentation. (b) Variations in lateral displacement of the indenter tip with time

Fig.5.5 showed the simulation result of the medium bond. Similar to the strong bond, the tip moved to the right at first. However, after reaching a rightmost point, the tip began to move back to the left-hand side, as Fig.5.5 (b) illustrates. Because of the hard phase, the resistance from the right side to the movement of the tip was smaller than that from the left side, which made the tip moved to the right side first. When the deformation resulting from indentation reached a critical value, the interfacial bonds were broken. As a result, the constraint from the left side decreased significantly. This made the tip move back to the left side. In Fig.5.5 (b), one may see that the tip finally moved back to the right side. This happened because the tip might touch the hard phase and its lateral movement was restricted to the right side only. Fig.5.6 illustrates different stages during

indentation process. At the first stage, there was little crack to take place, which made the tip move to the right side because of stronger constraint from the left side. Cracking occurred later, which made the tip move toward the left side. The tip eventually moved toward the right side because of the interfacial failure.

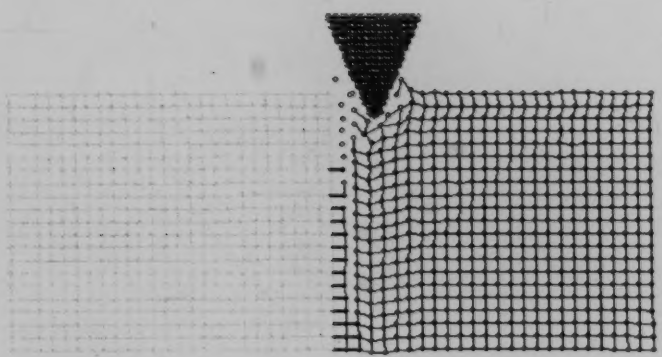

(a)

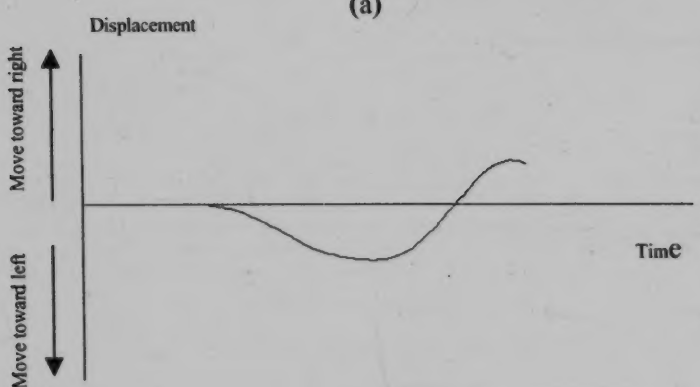

(b)

Fig.5.5 The simulation result for the medium interfacial bond. (a) Final simulation figure of indentation. (b) Variations in lateral displacement of the indenter tip with time

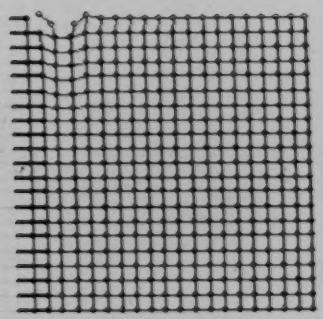

step = 110

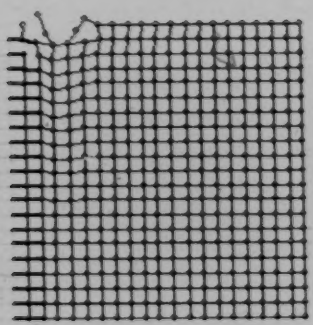

step = 160

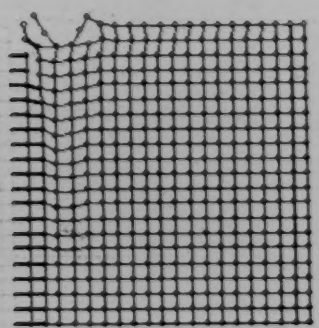

step = 210

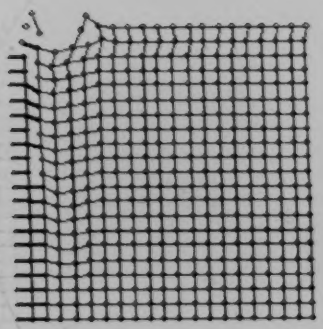

step = 260

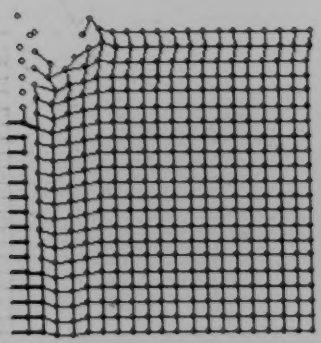

step = 330

Fig.5.6 Interfacial failure during indentation

For the weak bond, as Fig.5.7 (b) illustrates, the tip continuously moved to the left side during indentation. This happened because the interfacial bonds were weaker than the metal bonds, which were easy to be deformed and broken. Or in the other words, the lower constraint from the left side made the tip move to the left side continuously. Fig.5.7 (a) shows that many interfacial bonds were broken when the bonds were weak.

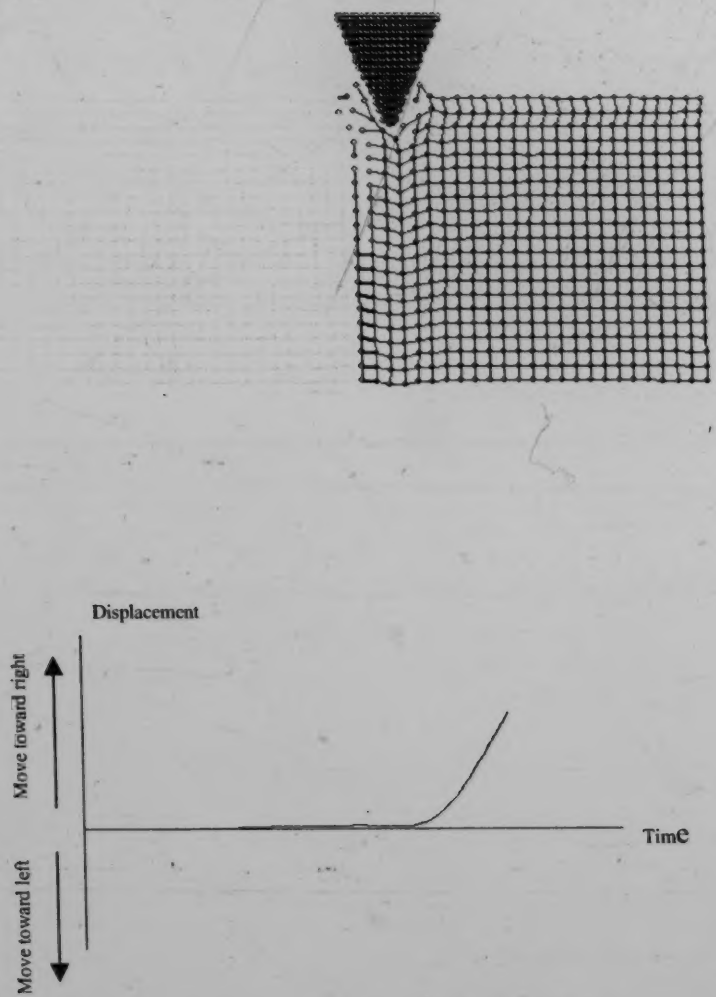

Fig.5.7 The simulation result for the weak interfacial bond. (a) Final simulation figure of indentation. (b) Variations in lateral displacement of the indenter tip with time

The results of the simulation are consistent with experimental observations. This largely supports the hypothesis that the interfacial debonding results in a change in the sign of the slope of the Fx – t curve during indentation.

5.2 Simulation of abrasive wear of pseudoelastic Composite material with nano-particles

5.2.1 Introduction

It has been demonstrated that the equi-atomic TiNi shape memory alloy exhibits high wear resistance benefiting from its pseudoelasticity and could be an excellent candidate for various tribological applications [60-62]. Pseudoelasticity is a special property of TiNi alloy, as depicted in Fig.5.8. When subject to a stress, TiNi alloy initially deforms elastically. When the stress reaches a high level, corresponding to the point A in Fig.5.8, phase transformation occurs, from an austenite phase (β) to a martensite phase (M). The alloy's deformation begins to behave "plastically". Within a certain range of such deformation, the "plastic" deformation may vanish if the stress is removed, because the martensitic phase can transform back to the austenite phase. This large strain recovery is called pseudoelasticity, resulting from a reversible phase transformation.

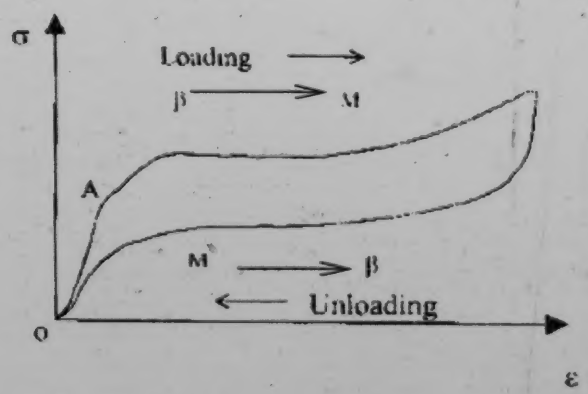

Fig.5.8 The Pseudoelasticity of TiNi alloy

Recent research work indicates that the wear resistance of pseudoelastic TiNi alloy can be considerably enhanced when hard particles, such as TiC, are added to the alloy [63]. The wear resistance of such a composite can be further improved by adding nano-TiN powder to its TiNi matrix [64]. The experimental results showed that a small amount of nano-TiN powder apparently improved the wear resistance of TiC/TiN composite. However, too much nano-TiN powder was detrimental to the composite. 5% nano-TiN turned to be the optimum amount.

Theoretical analysis using the finite element method had been made to investigate this situation. The result suggested that the integrated wear resistance of the TiNi matrix composite was not only influenced by the properties of individual phases but also by the interfacial bonding strength. However, the details about these factors are not very clear [65].

In order to further investigate the influence of TiN Nano-particles on the wear resistance of TiC/TiNi composite and to clarify the involved mechanism, the MSDM technique was applied to simulate sliding wear of this Nano-composite. As discussed in chapter 4, MSDM technique has been successfully applied to simulate and investigate the influence of reinforcing phase on wear of composite materials. The present modeling is an extension of the computational studies of composites with emphasis on the effects of nano particles on the wear behavior of a pseudoelastic composite.

5.2.2 Description of the modeling

The objective of this work is to apply MSDM technique to model abrasive wear of a TiNi composite material reinforced by TiC particles and nano-TiN powder. The

simulation is relatively complicated because two reinforcing phases need to be considered and the pseudoelasticity of the TiNi alloy matrix needs to be taken into account.

Fig.5.9 illustrate a sliding wear system consisting of nano-TiN/TiC/TiNi composite and a hard pin. The target has three phases: TiNi matrix, TiC reinforcing phase and TiN nano particles. Here, a nano TiN particle takes only one site. In order to simplify the model, both the bonds between TiC and the matrix and those

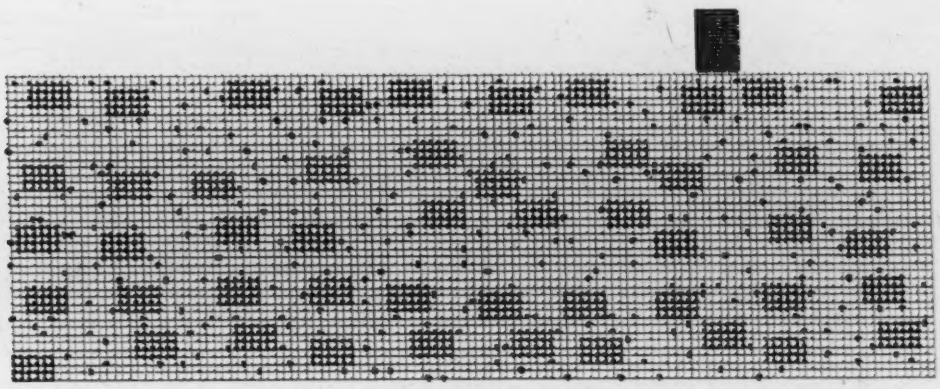

Fig.5.9 The schematic of a two-dimensional model for nano-TiN/TiC/TiNi composites

between nano TiN and the matrix are assumed to be elastic. It is assumed that there is no bond between two ceramic particles if they are in contact. During the sliding wear process, the pin consisting of 16X11 sites slid on the target surface. The pin was discretized and mapped using a lattice whose unit length was only half the unit length of the lattice for the target material. The site-site bonds of the pin were elastic and very strong, so that there was no damage to the pin during the wear process.

In order to simulate the sliding wear process, a constant load was uniformly added on the top of the pin. During wear, the pin moved to the left-hand side, scratching the surface of the target material with a constant velocity. The pin also penetrated into the target surface under the normal load. The process finished when the pin slid over a fixed distance in the direction parallel to the surface of the target material.

Details about dynamic simulation have been given in chapters 2,3 and 4. For the pseudoelastic TiNi matrix, its elastic modulus changes at different loads. Fig.5.10 schematically illustrates different strain ranges of a pseudoelastic TiNi matrix under tensile stress. As shown, the stress-strain curve of the matrix can be divided into four parts. From 0 to 12%, there are three strain stages, 0-1%, 1-8% and 8-12%, with different elastic moduli. In the range of 0-1%, only elastic deformation occurs in the material in β phase (ordered BCC), when strain exceeds 1%, a reversible martensitic transformation takes place, which provides a reversible strain up to 8%. When the strain is larger than 8%, the material is in a martensitic phase and it experiences elastic deformation until ε=12%. After ε>12%, plastic deformation of the martensitic phase takes place. If the total deformation exceeds 30%, the material will fail. The module for these four stages are determined by the slope of the $\sigma-\varepsilon$ curve. In order to investigate effects of the nano TiN powder on wear, four volume fractions of nano-TiN, 0%, 4%, 8% and 12%, were simulated. Mechanical properties of all materials involved in the modeling are listed in table 5.1.

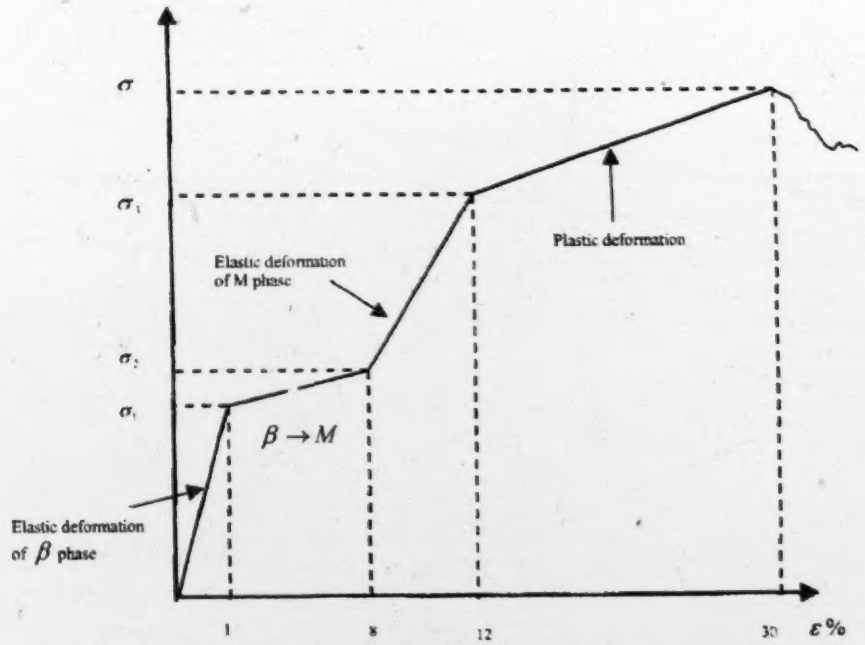

Fig.5.10 the schematic of four stages of stress-strain curve of pseudoelastic TiNi matrix

5.2.3 Simulation result

In this model, a reinforcing TiC particle occupied 8X8 = 64 sites. The volume fraction of TiC particles was 21%. A normal load of 5N was added uniformly on the top surface of the pin. Fig.5.11 illustrates cross-sectional pictures of worn samples containing 0%, 4%, 8% and 12% TiN nano particles, respectively. The simulation results indicate that the wear loss decreased initially with an increase in the volume fraction of the nano TiN particles. After reaching a minimum value, the wear loss increased as the volume fraction of the nano-TiN particles increased. This result was consistent with experiment observations [65] (see Fig.5.12).

Table 5.1 Mechanical properties of the materials under study

Material	Modulus $E(GPa)$	Yield stress or Maximum Stress $\sigma_y(MPa)$	Tensile strength $\sigma_T(MPa)$	Fracture strain $\varepsilon_f(\%)$
TiNi	40.0 (%0 - %1) 3.33 (1% - 8%) 6.67 (8% - 12%) (>12%)	400(%0 - %1) 633 (1% - 8%) 900 (8% - 12%) 1225	1225	30
TiN	248	496	496	0.2
TiC	483	966	966	0.2

The observed effect of nano TiN particles on the wear of the composite is understandable. The relative soft matrix was strengthened by the embedded hard nano-TiN particles. As shown, a small volume fraction of the nano-TiN particles reduced the wear damage to the composite. However, when too much nano-TiN powder was added, the composite became poor. This change was caused by an increase in the probability of the contact between nano-TiN particles and TiC reinforcing particles. Since there was no bond or weak bond between the ceramic particles, micro-cracking at the interfaces could be promoted under the wearing load. Hence the interfacial failure decreased the wear resistance of the composite. The current modeling well explains the effect of the volume fraction of nano TiN particles on wear of nano TiN/TiC/TiNi composite observed during experimentation.

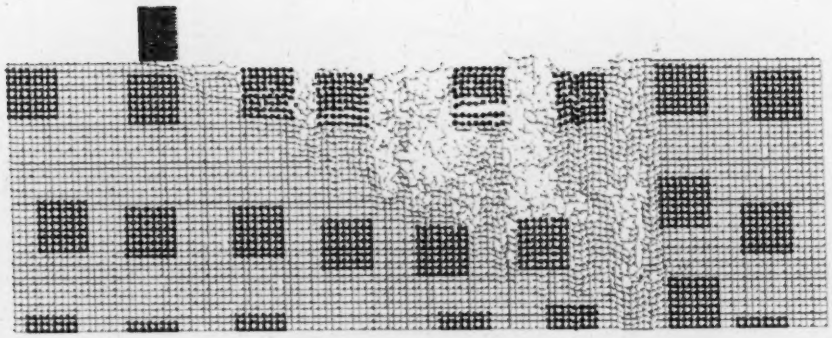

0% nano TiN

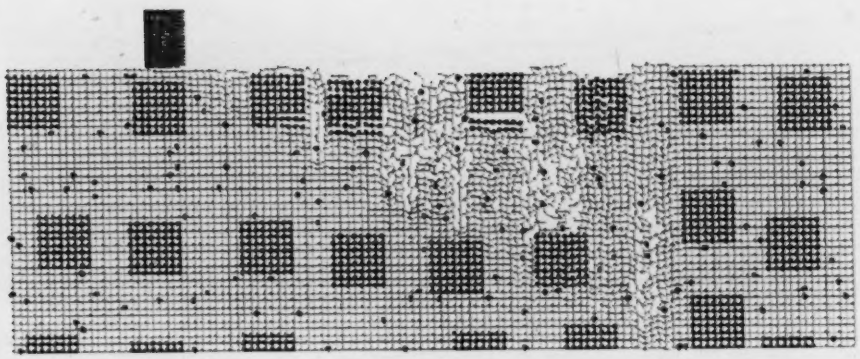

4% nano TiN

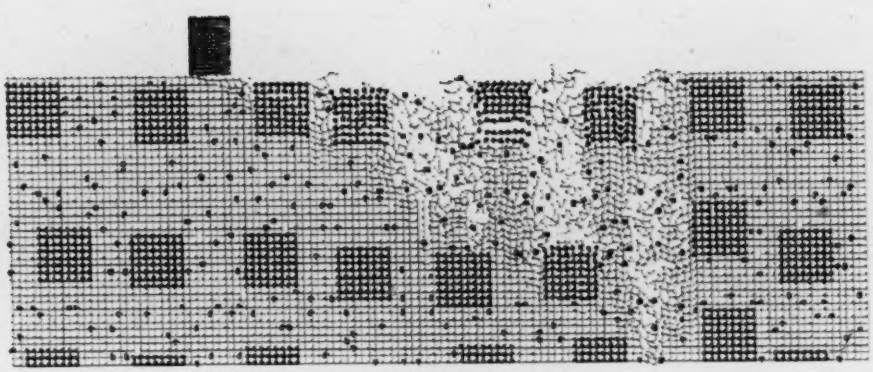

8% nano TiN

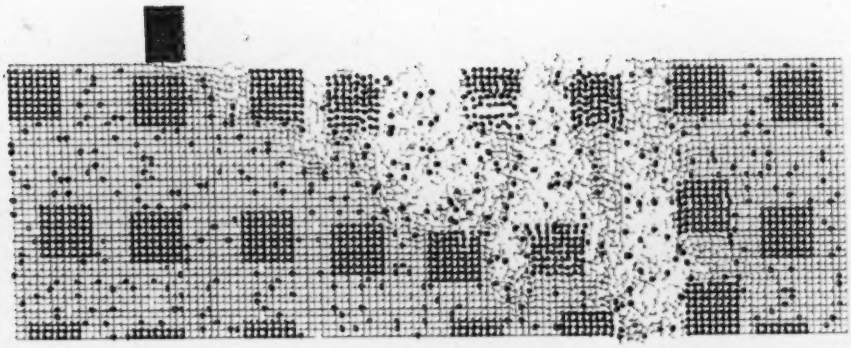

12% nano TiN

Fig.5.11 Sliding wear of 25% TiC/TiNi composites with different volume fractions of nano TiN particles

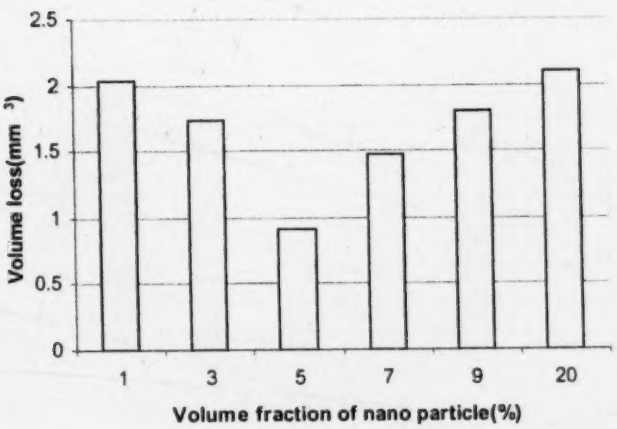

Fig.5.12 Volume losses of TiC/TiNi composites with different volume fractions of nano-TiN particles

5.3 Conclusion

Application of the MSDM technique was extended to investigations of interfacial debonding during indentation and the effect of nano particles on wear of a pseudoelastic

composite. Indentation near an interface was simulated using the MSDM technique to confirm the correlation between interfacial debonding and the change in sign of the slope of Fx – t curve. Influences of three interfacial bonds, strong, medium and weak, on indention curve were studied and the lateral displacement during indentation was computationally investigated.

Results of the simulation are consistent with experimental observations. Since the "computational experiment" was performed under controllable condition with a given bond strength, this consistence between simulation and experiment provides a support to the conclusion that the change in the sign of the slope of Fx~ t curve corresponds to interfacial debonding.

The MSDM technique was applied to investigate the influence of volume fraction of nano-TiN particles on the wear resistance of a TiC/TiNi composite. It was demonstrated that with an increase in the volume fraction of nano TiN particles, the wear resistance of the composite was improved. However, too much nano powder was harmful to the composite mainly due to the decrease in the interfacial adherence, since the probability for TiC particles to be in contact with nano TiN particles increased, which weakened the interface. The simulation results are consistent with experimental observations. This, in turn, demonstrates the effectiveness of the MSDM in investigation of material behavior during various processes.

Chapter 6

Conclusions and Future Work

6.1 Summary of the research results presented in different chapters

In this research, a computational model was developed, based on a micro-scale dynamic technique(MSDM), to model solid-particle erosion of materials. The model is described in chapter 2, including fundamentals of the MSDM and modification of the technique for erosion simulation.

Chapter 3 reports application of the erosion model in simulation of solid-particle erosion of homogenous materials. In this work, influences of impact angle, impact velocity, shape, rotation angle of erodent particles on erosion process were investigated. Crack propagation in the brittle material under impact of erodent particles with different front angles was also studied. Good agreement between the simulation results and experiment observations was found.

In chapter 4, the application of the erosion model to simulate solid-particle erosion of composite materials is reported, with the emphasis on the effect of microstructure on erosive damage. In this work, various factors on erosion of composite were investigated, including effects of the volume fraction of reinforcing phase, interfacial bonding, erodent size, and the size ratio of the erodent to the reinforcing particles. It was demonstrated that the model was effective for investigating the mechanism responsible for erosion of materials and help to establish the relationship between the microstructure of a material and its wear behavior. The model allows visualizing the erosion process. Such a capability would help us to obtain information on the failure mechanism in detail.

Chapter 5 reports extended applications of MSDM technique in other areas. Interfacial failure of interfaces in composite was modeled with the aim of studying

the correlation between interfacial debonding and changes in the lateral force. In this work, responses of strong, medium and weak interfacial bonds to indentation were studied and changes in the lateral displacement of the indenter tip with time were investigated. The simulation results were consistent with experiment observations, which provides a support to the hypothesis that the change in the sign of the slope of Fx~ t curve corresponds to interfacial debonding.

The MSDM technique was also applied to investigate the influence of volume fraction of TiN nano-particles on the wear resistance of a TiC/TiNi composite. It was demonstrated that with an increase of the volume fraction of TiN particles, the wear resistance improved at first. After reaching a critical point, the wear resistance decreased. The simulation results are consistent with experiment data and well explain the observed phenomena. This part of work is also presented in chapter 5.

The entire the procedure of modeling erosion of materials is summarized by the following chart (Fig.6.1).

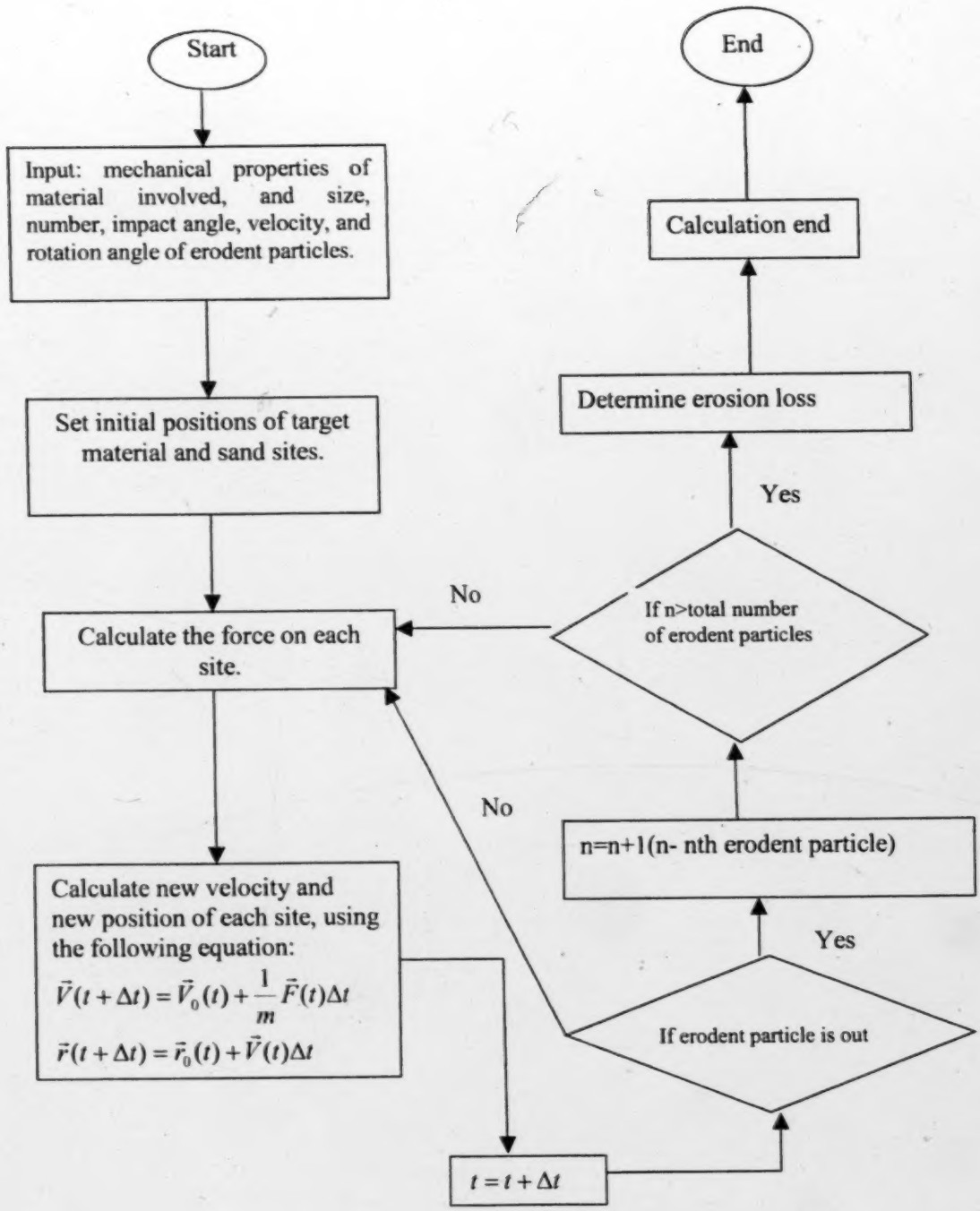
Start
Input: mechanical properties of material involved, and size, number, impact angle, velocity, and rotation angle of erodent particles.
Set initial positions of target material and sand sites.
Calculate the force on each site.
Calculate new velocity and new position of each site, using the following equation:
$\vec{V}(t+\Delta t)=\vec{V}_0(t)+\frac{1}{m}\vec{F}(t)\Delta t$
$\vec{r}(t+\Delta t)=\vec{r}_0(t)+\vec{V}(t)\Delta t$
$t=t+\Delta t$
If erodent particle is out
No
n=n+1(n- nth erodent particle)
If n>total number of erodent particles
No
Yes
Determine erosion loss
Calculation end
End
Yes

Fig.6.1 A flow chart of the MSDM

6.2 Future work

1) Effects of multiple impact and erodent size distribution on erosion

Erodent flow has great influence in erosion damage. In reality, erodent particles usually have different sizes with a size distribution. In addition, many erodent particles may impinge the target material simultaneously. In the present study, only erosion caused by erodent particles having the same size was modeled. The erodent particles were ejected one by one to attack the target material at random positions. This assumption may influence the accuracy of simulation. In the future work, multiple impact and size distribution of erodent particles would be taken into account.

2) Effects of shapes of the reinforcing phase and erodent particles on erosion

The shape of reinforcing phase has great influence on wear process due to the increased stress concentration at the edge of each reinforcing particle. However, in the present work, only rectangle reinforcing particles having the same size were considered for each wear process. In realistic composite materials, reinforcing particles may have different shapes. Future work would include studies of effects of the shape of reinforcing particles on erosion. In addition, effects of the size distribution of reinforcing particles having different shapes would also be studied.

3) 3-D model

In present model, modeling was carried out in a 2-D space. It is expected that a 3-D model would provide more details regarding the solid-particle erosion. For example, for

2-D modeling, the wearing stress is different from that in a 3-D space, which decreases the accuracy of modeling. 3-D modeling would be certainly necessary if one wishes to develop the present model for quantitative tribological research and application.

4) Determination of the time interval and initial length of bond

In the present work, the time interval Δt was selected in a "safe" range. It is not convenient because this range might vary under different erosion conditions. This is also a barrier for using the MSDM to obtain absolute erosion loss. Based on our experience of the study, the time interval should be related to many factors, such as impact velocity, density, initial length and fracture length of impact erodent and target material. In the future work, the relationship between Δt and these factors could be investigated.

5) Extension of MSDM technique for modeling other types of wear

In present work, the MSDM has been demonstrated effective for studying erosion, abrasive wear, indentation and crack propagation. In industrial environment, however, wear may occur in other failure modes, such as corrosion and oxidation. Incorporating environmental effect in the model would be one of future main tasks.

Publications based on this work

[1] Q.Chen, D.Y.Li, Computer simulation of solid-particle erosion, Wear, 2002, in press

[2] Q.Chen, D.Y.Li, Computer simulation of solid-particle erosion of composite materials, Wear of Materials, 2002, Accepted

[3] H.Zhang, Q.Chen, D.Y.Li, New method for the measurement of interfacial bonding strength by using indentation lateral force test, submitted to Metall.Mater.Trans, 2003

References

1. Standard terminology related to erosion and wear; Annual Book of Standards, No2, ASTM, Philadelphia, PA, 1993.
2. M.B.Peterson, W.O.Winer, Wear Control Handbook, ASME, New York, 1980.
3. Ernest Rabinowicz, Friction and Wear of Materials, 2nd ed., John Wiley & Sons, Inc., (1995).
4. Associate community on tribology, NRC Canada, report no.26556, 1986.
5. H.C.Meng, K.C.Ludema, Wear models and predictive equations: their form and content, Wear 181(1995)443-457.
6. R.O.Scattergood, Review of Erosion Test Methodologies, Paper No.5, Proc.Corrosion-Erosion-Wear of Materials at Elevated Temperatures(Berkeley, CA), Jan 1990.
7. I.Finnie, The mechanism of erosion of ductile metals, Proc.3rd U.S.Nat.Congr.Applied Mechanism, ASME, New Yourk, 1958, 527-532
8. I.Finnie, Erosion of surface by solid particles, wear, Vol.3, 1960, 87-103
9. J.G.A.Bitter, A study of erosion phenomena, Parts 1,2, Wear, Vol. 6, 1963, 5-21
10. J.H.Neison, A.Gilchrist, Erosion by a stream of solid particles, Wear, Vol. 11, 1968, 111-122
11. E.Raask, Tube erosion by ash impaction, Wear, Vol. 13, 1969, 301-315
12. G.P.Tilly, Erosion caused by airborne particles, Wear, Vol. 14, 1969, 63-79
13. W.J.Head, M.E.Harr, The development of a model to predict the erosion of materials by natural contaminates, Wear, Vol. 15, 1970, 1-46
14. G.P.Tilly., A two stage mechanism of ductile erosion, Wear, Vol.23, 1973, 87-96

15. I.M.Hutchings, A model for the erosion of metals by spherical particles at normal incidence, Wear, vol.70, 1981, 269-281

16. A.V.levy., The erosion of metal alloys and their scales. Proc.NACE Conf. Corrosion-Erosion-Wear of Materials in Emerging Fossil Energy Systems, 1982, 298-376

17. A.V.levy., The solid particle erosion behavior of steel as a function of microstructure, Wear, Vol. 68, 1981, 269-287

18. K.Schimizu, T.Noguchi, Y.Matubara., FEM analysis of erosive wear, Int.J.Cast Metals Res., 1999, 11, 515-520

19. Y.Gachon,A.B.Vannes, G.Farges, Study of sand particle erosion of magnetron sputtered multilayer coatings, International Conference on Erosive and Abrasive Wear (ICEAW); 9th International Conference on Erosion by Liquid and Solid

20. K.Shimizu, T.Noguchi, H.Seitoh., FEM analysis of the dependency on impact angle during erosive wear, International Conference on Erosive and Abrasive Wear (ICEAW); 9th International Conference on Erosion by Liquid and Solid Impact (ELSI IX), Cambridge, UK, 1998

21. P.J.Woytowitz, R.H.Richman., Solid mechanics modeling of erosion damage, ASTM (USA), 1997, 186-199

22. P.J.Woytowitz, R.H.Richman., Modeling of damage from multiple impacts by spherical particles, Wear, vol. 233-235, 1999, 120-133

23. G.L.Sheldon, I,Finnie., The mechanism of material removal in the erosive cutting of brittle materials, J.Eng.Ind., Vol.88, 1966, 393-400

24. A.G.Evans, M.E.Gulden, Impact damage in brittle materials in the elastic-plastic response regime, Proc.R.Soc.A, Vol.361, 1978, 343-365

25. G.Sundararajan., The solid particle erosion of metallic materials: the rationalization of the influence of material variables, Wear, vol. 186-187, no. 1, July 1995, 129-144

26. B.F.Levin, K.S.Vecchio, J.N.DuPont, Modeling solid-particle erosion of ductile alloys, Metallurgical and Materials Transactions A , vol. 30A, no. 7, 1999, 1763-1774A

27. K.C.Ludema., Wear, in:Friction, Wear, Lubrication, A Textbook in Tribology, CRC Press, Boca Raton, 1996

28. H.S.Meng, K.C.Ludema., Wear life equations for mechanical designers: state of the art, 1993 International Wear of Materials Conference, San Francisco, 1993

29. M.O.Robbins, J.Kirm, Energy dissipation in the interfacial friction, MRS Bulletin, Vol.23, 1998, 23-26

30. P.Gumbsch, R.M.Cannon., Atomic aspects of brittle fracture, MRS Bulletin, Vol.25, No.5, May 2000, 15-20

31. G.E.Beltz, D.M.Lipkin., A dislocation model for the directional anisotropy of grain-boundary fracture, MRS Bulletin, Vol.25, No.5, May 2000, 21-26

32. J.A.Harrison, S.J.Stuarat, D.W.Brenner, Atomic-scale simulation of tribological and related phenomena, Handbook of Micro/Nanotribology, 1998

33. D.Y.Li, K.Elalem, M.J.Anderson., A microscale dynamical model for wear simulation, Wear, Vol.225, 1999, 380-386

34. K.Elalem, D.Y.Li., Dynamic simulation of an abrasive wear process, Journal of Computer-Aided Materials Design, 6,1999, 185-193

35. K.Elalem, D.Y.Li., Dynamic simulation of abrasive wear of composite materials, Advances in Powder Metallurgy and particulate Materials, Vol. 3, 11, 1999, 3-12

36. R.Winter, I.M.Hutchings., The role of adiabatic shear in solid particle erosion, Wear, Vol.34, 1975, 141-148

37. P.Shewmon., Particle size threshold in the erosion of metals, Wear, Vol.68, No.2, 1981, 253-258

38. W.D.Callister, Jr, Materials Science and Engineering An Introduction, Fourth Edition, 1997

39. P.J.Blau et al, ASM Handbonk, Vol.18, Friction, Lubrication, and Wear Technology, ASM International, 1992

40. A.G.Evans, T.R.Wilshaw, Quasi-static solid particle damage in brittle solids. Pt. 1. observations, analysis and implications, Acta Metall., 24 (10)(1976) 939-956

41. P.Ostojic, R.McPherson, A review of indentation fracture theory: its development, principles and limitations, International Journal of Fracture, 33(1987) 297-312

42. P.K.Rohatgi, Friction and wear technology for advanced composite materials, ASM International, Materials Park, Ohio, 1994

43. H.Z.Ye, D.Y.Li, R.Eadie, Development of new wear-resistant material: TiNi-based composite, Ph.D. Thesis, University of Alberta, 2002

44. A.J.Ninham, and A.V.Levy, The erosion of carbide-metal composites, Wear, 121(1988) 347

45. F.S. Shieu, M.H. Shiao, Measurement of the interfacial mechanical properties of a thin ceramic coating on ductile substrates, Thin Solid Film, 306 (1997) 124-129.

46. C.Q Liu, M.S. Li, Z.J. Jin, W.T. Wu, Tensile and adhesive strengths of fine TiN film on Ti substrate, Acta Metqllurfica Sinica, Series B: Process metallurgy and Miscellaneous, 6B(1993)126-129.

47. Xie Ming, Karbhari Vistasp M, Peel test for characterization of polymer composite/concrete interface, Journal of Composite Materials. v 32 n 21 1998, p 1894-1913.

48. P.J. Burnett, D.S. Rickerby, The scratch adhesion Test: an elastic-plastic indentation analysis, Thin Solid Film, 157 (1988) 233-254

49. Lux. T, Adhesion of copper on polyimide deposited by arc-enhanced deposition, Surface and coatings technology, 133-134(2000)425-429.

50. H. Ollendorf, D. Schneider, A comparative study of adhesion test methods for hard coatings, Surface and Coatings Technology, 113(1999) 86-102.

51. J. Yuan and V. Gupta, Measurement of interface strength by the modified laser spallation technique. I. Experiment and simulation of the spallation process. 74 (1993) 2388-2396.

52. M.V. Swain and J. Mencik, Mechanical property characterization of thin films using spherical tipped indenters, Thin Solid Films 253(1994)204

53. S. V. Hainsworth, M. R. McGurk, T.F. Page, The effect of coating cracking on the indentation response of thin hard-coated systems, Surface coatings and technology, 102(1998) 97-107

54. Y.Lu, D.M.Shinozaki, Microindentation induced debonding of polymer thin films from rigid substrates, Journal of Materials Science, 37(2002)1283-1293.

55. J.Bystrzycki, J. Paszula, R. Rrebinski, The microstructure and interface behaviour of Ni/NiAl composites produced by the explosive compaction of powders, Journal of Materials Science, 29(1994) 6221-6226.

56. W.J.Fan et al., Roll-bonding of a laminate Al alloy/Ni3Al-type alloy composite, Z.Metallkd. 85(1994) 7, 522-527.

57. D.Chicot et al. Apparent interface toughness of substrate and coating couples from indentation tests, Thin solid films 283(1996) 151-157.

58. P.H. Demarecaus, D.Chicot, J. Lesage, Interface indentation test for the determination of adhesive properties of thermal sprayed coatings, Journal of materials science letters 15(1996) 1377-1380

59. H.Zhang and D.Y.Li, presented at 14th Canadian Materials Science Conference, 2002

60. Ball, A, On the Importance of Work Hardening in the Design of Wear-Resistant Materials, Wear, 91 (1983) 201- 207

61. R.H.Richman, A.S.Rao, D.Kung, Cavitation erosion of NiTi explosively welded to steel, Wear 181-183 (1995) 80 – 85

62. D.Y.Li, A new type of wear-resistant material: pseudo-elastic TiNi alloy, Wear, 221 (1998) 116 – 123

63. H.Z.Ye, R.Liu, D.Y.Li and R.Eadie, Development of a new wear-resistant material: TiC/TiNi composite, Scripta Mater., 41 (1999) 1039

64. Y.C.Luo, D.Y.Li, New wear-resistant material: Nano-TiN/TiC/TiNi composite, Journal of Materials Science (USA), 36 (2001) 4695-4702

65. Y.C.Luo, R.Liu, D.Y.Li, Investigation of the mechanism for the improvement in wear resistance of nano-TiN/TiC/TiNi composite: a study combining experiment and FEM analysis, Materials Science and Engineering A (Switzerland), 329-331 (2002) 768-773